An exploration of the molecular mechanisms underlying the effects of hyperglycaemia on the autorrhythmicity of cardiac-like stem cells

By

Amanda Menzele
MNZAMA005

Supervisor: A/Prof. Asfree Gwanyanya

SUBMITTED TO THE UNIVERSITY OF CAPE TOWN
In fulfilment of the requirements for the degree
MM095 MSc Med (by dissertation)
HUB 5004W
Department of Human Biology
Faculty of Health Sciences
UNIVERSITY OF CAPE TOWN

Date of submission: 16 September 2022

Declaration

I, Amanda Menzele, hereby declare that the work on which this dissertation/thesis is based is my original work (except where acknowledgements indicate otherwise) and that neither the whole work nor any part of it has been, is being, or is to be submitted for another degree in this or any other university.

I empower the university to reproduce for the purpose of research either the whole or any portion of the contents in any manner whatsoever.

Signature: Signed by candidate

Date: 29 September 2023

Acknowledgements

I wish to express my sincerest gratitude to my supervisor and mentor, Dr Asfree Gwanyanya, for his ongoing support throughout my budding career as a young clinician scientist.

Thank you to my colleagues, Hamida Aboalgasm and Nikhil Amtha. I would not have come this far without your patience and guidance.

I would like to thank my sponsors, particularly the National Research Foundation, for their financial support.

To the Oprah Winfrey Leadership Academy for Girls, thank you for shaping me into the young woman I am today.

To Ms Susan Norval, thank you for always being there and for always making a plan.

Finally, I wish to thank my family for giving me wings to fly. To “mimom”, thank you for always believing in my dreams and always putting us first.

And to my late grandmother, Faith Nomonde Menzele, I hope I have made you proud *Khulu*.

***

Table of Contents

List of figures

List of abbreviations

mESC: mouse embryonic stem cell

iMEFs: inactivated mouse embryonic fibroblasts

EB: embryoid body

DMSO: dimethyl sulfoxide

DMEM: Dulbecco's Modified Eagle Medium

SA node: sinoatrial node

HCN: hyperpolarization-activated cyclic nucleotide-gated channel

I_f: '*funny current*'

Na^+: sodium ion

K^+: potassium ion

Ca^{2+}: calcium ion

KCl: potassium chloride

SR: sarcoplasmic reticulum

Cx: connexin

cAMP: cyclic adenosine monophosphate

TGF-$\beta 1$: Transforming growth factor beta, isoform 1

ECG: electrocardiogram

GJIC: gap junction intercellular communication

LY: Lucifer yellow

Abstract

Introduction

Diabetes mellitus with uncontrolled hyperglycaemia is a major risk factor for heart rhythm disturbances. Hyperglycaemia during pregnancy is particularly concerning, as offspring of poorly controlled diabetic mothers are at an increased risk of developing life-long serious cardiovascular complications. Although structural abnormalities such as congenital heart defects and hypertrophic cardiomyopathy are by far the most common sequelae in these infants, it is becoming increasingly apparent that a vulnerability towards malignant dysrhythmias is far more prevalent than generally reported in the literature. Unfortunately, the mechanistic link between hyperglycaemia and impaired foetal cardiac electrophysiology is poorly understood. Using a cardiac developmental cellular model, this study aimed to explore the effects of hyperglycaemia on the autorrhythmicity of mouse embryonic stem cell (mESC)-derived cardiac-like cells.

Methods

mESCs were differentiated into cardiac-like cells through embryoid body (EB) formation, in culture medium containing either baseline (25 mM) glucose- or high (50 mM) glucose concentrations. Time-lapse images of spontaneously pulsatile EBs were captured on an EVOS™ M5000 imaging system and analysed using a motion-detecting macro on ImageJ, Myocyter™, for the assessment of rate and rhythm. EB beating response to β-adrenergic drug isoprenaline, as well as hyperpolarization-activated cyclic nucleotide-gated (HCN) channel blocker ivabradine, was assessed. The frequency of ectopic beats was recorded before and after the application of pro-arrhythmogenic drug potassium chloride. Sensitivity to a multi-channel blocker quinidine was assessed by determining the onset of asystole. Gap junction intercellular communication (GJIC) was evaluated using scrape-loading lucifer yellow dye transfer. Molecular analysis of key proteins involved in cardiac pacemaking, and impulse propagation was carried out using Western blot analysis and immunocytochemistry. These included the major cardiac gap junction protein connexin (Cx)-43, as well as the dominant HCN channel isoform in the mammalian heart, HCN4. To provide mechanistic insights, the expression of transforming growth factor beta 1 (TGF-β1) and its downstream

effector, phosphorylated (p)- Smad3, were analysed using immunoblot assays. A *p*-value of 0.05 was used as the threshold for statistical significance.

Results

Pluripotent mESCs were successfully differentiated into pulsatile cardiac-like cells that stained positively for the cardiac sarcomeric protein α-actinin2 and cardiac gap junction protein Cx43. High glucose suppressed mESC cardiac differentiation, as evidenced by the significantly lower proportion of spontaneously beating EBs in this group. Furthermore, high glucose suppressed cardiac pulsatile activity, as was shown by the significantly reduced EB beating rate. This suppressed autorrhythmicity could not be readily explained by the modulation of the cardiac pacemaker channels, as neither HCN channel expression nor EB beating response to ivabradine or isoprenaline were altered by high glucose. The frequency of baseline and inducible ectopic beats was not significantly different between the two glucose groups, however the time to quinidine-induced asystole was significantly shorter in high glucose EBs. High glucose impaired GJIC, as shown by the reduced lucifer yellow dye transfer distance and decreased the expression of Cx43 at protein level. Finally, the protein expression of TGF-β1 or phosphorylated-Smad3 was significantly increased by high glucose.

Discussion and conclusion

High glucose suppressed the autorrhythmicity and gap junction-mediated impulse propagation of mESC-derived cardiomyocytes. High glucose also enhanced cellular sensitivity to a multi-channel blocker quinidine and increased propensity to asystole, the most severe form of dysrhythmia. The underlying mechanisms likely involve activation of the TGFβ1/Smad3 signalling cascade. These findings provide new insights into the proarrhythmic effects of hyperglycaemia on the developing heart, with possible clinical implications for diabetic foetal cardiac disease.

***

Chapter 1: Introduction and literature review

1.1 Diabetes mellitus and cardiovascular disease

Diabetes mellitus is a growing non-communicable epidemic, with an estimated global prevalence as high as 536 million adults in 2021 (Ogurtsova *et al.*, 2022). It is a metabolic disease typically characterised by inappropriately high blood glucose levels (hyperglycaemia) because of a lack of insulin or resistance to insulin (Skyler, 2004). Type 1 diabetes mellitus, which typically presents in children, is the result of autoimmune destruction of the insulin-secreting pancreatic β-cells, resulting in an absolute deficiency of the hormone insulin, and thus an inability to maintain normal plasma glucose levels (Guthrie and Guthrie, 2004). Type 2 diabetes mellitus, which accounts for nearly 90% of all cases of diabetes, involves a more complex interplay between genetic and lifestyle factors. The underlying pathology in type 2 is that of insulin resistance resulting in a *relative* deficiency of this hormone, and thus impaired blood glucose regulation (Guthrie and Guthrie, 2004). The onset of type 2 diabetes is typically in adulthood, and it is often associated with obesity, dyslipidaemia and hypertension, a cluster of disorders known as the metabolic syndrome (Aganović and Dušek, 2007). The other type of diabetes mellitus is called gestational diabetes, which manifests itself for the first time during pregnancy, and it is thought to be the result of pancreatic β-cell dysfunction on a background of underlying insulin resistance (Plows *et al.*, 2018). Patients with gestational diabetes are at an increased risk of subsequently developing type 2 diabetes later in life. Other infrequent forms of diabetes, which account for less than 1% of all diabetics, include rare genetic disorders and endocrinopathies (Lee and Huda, 2021). Regardless of the specific type of diabetes mellitus, a universal feature of the disease that is also responsible for most diabetic complications is the presence of hyperglycaemia (Skyler, 2004). As such, the diagnosis of diabetes is made when blood glucose levels exceed a certain threshold, with 11 mmol/L being the absolute cut-off for a randomly collected sample in an unfasted patient. Similarly, monitoring of diabetes and response to treatment relies primarily on assessing glycaemic control.

Although diabetes was previously regarded as a “disease of affluence”, it has now been shown that nearly four-fifths of the diabetic population reside within low-and middle-

income countries (Dunachie and Chamnan, 2019). Therefore, diabetes imposes a considerable economic burden in these resource-limited settings, where the annual cost of treating diabetes has been estimated to be as high as $3.3 billion in the Sub-Saharan region alone (Mapa-Tassou *et al.*, 2019). A substantial proportion of this expenditure goes towards treating the complications of diabetes, which are debilitating and affect nearly every organ system in the body, including the renal, neurological, and cardiovascular systems.

Of all these complications, cardiovascular disease is the main contributor to morbidity and mortality (Einarson *et al.*, 2018). Although coronary artery disease and heart failure exert the heaviest toll on diabetic patients, a common endpoint of these pathological processes is the occurrence of heart rhythm disturbances (Grisanti, 2018). Diabetic patients are disproportionately affected by potentially life-threatening arrhythmias, including atrial fibrillation, ventricular tachycardia, and sick sinus syndrome requiring pacemaker replacement (Lear *et al*., 1996; Agarwal and Singh, 2017). The presence of these arrhythmias predisposes to heart failure and sudden cardiac death; however, the exact pathophysiological mechanisms remain unclear (Grisanti, 2018). This is in part due to the complex and multifactorial nature of diabetes, with numerous metabolic derangements such as hyperglycaemia, impaired insulin signalling, dyslipidaemia and electrolyte imbalances all playing a key role in its pathogenesis (Ogedengbe and Ezeani, 2014). Of all these metabolic abnormalities, however, hyperglycaemia alone has been identified as the key initiator of cardiovascular complications in this patient population (Mapanga and Essop, 2016). A recent meta-analysis revealed a dose-dependent relationship between blood glucose levels and the risk of cardiac arrhythmias in diabetics (Aune *et al.*, 2018), further highlighting the central role of hyperglycaemia in the pathogenesis of diabetic cardiac complications.

Hyperglycaemia during pregnancy is particularly concerning, because its clinical implications are far-reaching and extend beyond the mother, to affect the offspring as well. Infants born to diabetic mothers are at a great risk of developing life-long serious cardiovascular complications such as congenital cardiac defects, hypertrophic cardiomyopathy, and malignant dysrhythmias through a process known as foetal cardiac remodelling (Akbariasbagh *et al*., 2017; Hoodbhoy *et al*., 2019; Hornberger, 2006). Although the structural cardiac abnormalities account for the vast majority of cardiovascular sequelae in

these infants (Shankar *et al.*, 2019), it is becoming increasingly apparent that heart rhythm disturbances are far more prevalent than generally reported (Pike *et al*., 2013). Furthermore, *in utero* exposure to hyperglycaemia may cause long-lasting alterations to the electrophysiological properties of the developing heart, which, because they are not as readily detectable as the structural defects, may go undiagnosed until much later in life, when several other cardiovascular risk factors have come into play. Unfortunately, the effect of hyperglycaemia on cardiac electrophysiology is poorly understood, and what limited data there is, is based on the adult diabetic heart, in which cardiomyocytes are terminally differentiated and have lost their proliferative capacity (Lázár *et al*., 2017). As such, the findings from these studies cannot be readily extrapolated to the developing heart, which leaves a considerable gap in our current understanding of how maternal diabetes creates a substrate for arrhythmias in the foetal heart.

The study of foetal cardiac remodelling has been hampered by a lack of suitable experimental models. Previously, studies have relied on isolated neonatal rat cardiomyocytes (du Pré *et al*., 2017), the use of which is limited by their low yield and proliferative capacity, as well as their relatively short lifespan *in vitro*. More recently, mouse embryonic stem cell (mESC)-derived cardiac-like cells have emerged as a suitable model for studying cardiac developmental pathology at the cellular level (Czechanski *et al*., 2014). They display spontaneous pulsatile activity *in vitro*, making them well-suited to the study of arrhythmogenesis in the developing heart. Previous studies using this cardiac cellular model have shown that hyperglycaemia impairs cardiac differentiation of mESCs and causes cardiomyocyte contractile dysfunction through myofilament disruption (Yang *et al.*, 2016; Aboalgasm *et al.*, 2021). The effect of hyperglycaemia on the autorrhythmicity of these spontaneously beating cells, however, remains largely unknown. The purpose of the current study was to therefore characterise the beating characteristics of mESCs-derived cardiac-like cells grown under high glucose conditions, and to explore possible underlying mechanisms by which diabetes may produce arrhythmias in the developing heart.

1.2 Cardiac rhythm and effects of diabetes

1.2.1 The physiology of cardiac autorrhythmicity

Cardiac autorrhythmicity refers to the unique ability of the heart to generate rhythmic action potentials and initiate its own contractions without any external stimulus (Mangoni and Nargeot, 2008). This automatic electrical activity arises from specialised pacemaker cells found at various sites along the conduction system of the heart. In the mammalian heart, the sinoatrial (SA) node, which is located in the upper part of the right atrial wall, is considered to be the primary or natural cardiac pacemaker *(Choudhury et al*.,2015). The other specialised structures that can initiate the cardiac impulse include the atrioventricular (AV) node and the Purkinje fibres. Under normal physiological conditions, the automaticity of these subsidiary or "back-up" pacemakers is suppressed by the faster intrinsic firing rate of the SA node, a phenomenon known as the hierarchy of pacemaker function (Mangoni and Nargeot, 2008). In the setting of pathological states such as heart block and cardiac failure, the AV node and Purkinje network may assume the role of the dominant pacemaker (Janse, 2004).

The specialisation of all pacemaking cells can be attributed, in large part, to their differential expression of certain ion channel genes which are involved in the generation of cardiac automaticity (Mangoni and Nargeot, 2008). Among these, the hyperpolarization-activated cyclic nucleotide-gated (HCN) ion channels have been identified as key players in the generation of the cardiac action potential (DiFrancesco, 1985). The HCN family consists of four different isoforms (HCN1-4), with HCN4 being the dominant isoform expressed within the mammalian SA node (Sartiani *et al.*, 2017). The HCN channels conduct the "funny current" or I_f, which is so named because of its unique ability to initiate a net inward current of Na^+ and K^+ ions at hyperpolarised membrane potentials of -60 to -50mV (DiFrancesco, 1991). This gradual accumulation of positive charge within the cell interior brings about the diastolic depolarisation phase, which is unique to the pacemaker action potential. As the pacemaker cells begin to depolarise and the membrane potential becomes less negative, there is activation and recruitment of other inward currents, ultimately reaching the threshold for an action potential (Mangoni and Nargeot, 2008).

The intrinsic heart rate, which is determined by the primary pacemaker of the heart, is under constant modulation by the autonomic nervous system. To this end, HCN channel activation is directly regulated by intracellular cyclic adenosine monophosphate (cAMP), which, in turn, is increased by β-adrenergic stimulation from sympathetic nerves and decreased by muscarinic agonists from the parasympathetic nerves (Sartiani *et al.*, 2017). Other possible regulatory mechanisms of HCN channel activity include ancillary subunits, microRNAs, and kinase-mediated phosphorylation, although the role of these is not clearly understood (D'Souza *et al.*, 2017; Yang *et al.*, 2020)

Although I_f plays a key role in pacemaking, several other ionic and cellular mechanisms contribute a great deal to cardiac automaticity. This is evidenced by the observation that pharmacological inhibition of HCN channels with blockers such as ivabradine and caesium slows down spontaneous beating rate but does not completely abolish cardiac pacemaking (Kennedy *et al.*, 1993). Of particular importance to the generation of spontaneous depolarization within the SA node, is the rhythmic release of intracellular Ca^{2+} from the sarcoplasmic reticulum (SR) via the ryanodine receptor. This is what is commonly referred to as the "Calcium clock", and it is thought to play an important part in the late phase of diastolic depolarisation (Joung *et al.*, 2009). The increase in membrane potential initiated by I_f causes activation of T-type Ca^{2+} channels, which are activated at relatively lower voltages compared to other voltage-gated Ca^{2+} channels (Ziad and Miller, 2019). This initial Ca^{2+} influx triggers localised release of Ca^{2+} from the SR into the cytosol, which drives the Na^{+}-Ca^{2+} exchanger, resulting in a further increase in the membrane potential. Eventually, the L-type Ca^{2+} channels are activated at approximately -40mV, resulting in a much larger scale, whole-cell depolarization known as an action potential (Joung *et al.*, 2009). The pharmacological inhibition of these SR-mediated Ca^{2+} transients results in a prolongation of diastolic depolarisation and a slowing of the spontaneous firing rate of the pacemaker, similar to what is observed when I_f is inhibited (Bucchi *et al.*, 2003). The main regulatory mechanism of these Ca^{2+}-handling proteins, particularly the L-type Ca^{2+} channels, is through phosphorylation by protein kinase A (PKA) and Ca^{2+}/calmodulin-dependent protein kinase II (CaMKII) (Joung *et al.*, 2009). Importantly, the calcium clock is modulated by β-adrenergic stimulation in several ways. Firstly, through enhanced localised Ca^{2+} release via the

ryanodine receptor, resulting in acceleration of the rate of diastolic depolarisation (Vinogradova *et al*., 2002). Secondly, through intracellular cAMP-mediated activation of PKA, which, in turn, enhances L-type Ca^{2+} currents (Mangoni and Nargeot, 2008). The involvement of intracellular Ca^{2+} signalling in the generation of the heart rhythm is a relatively new concept (Rubenstein and Lipsius, 1989), and as such, not a great deal is understood about its role in certain cardiac pathological states.

The generation of the cardiac action potential within the pacemaker is just one aspect of autorrhythmicity. The propagation of this electrical impulse within the pacemaker, and then beyond, through the conduction pathways of the heart is equally important to maintaining a normal cardiac rhythm (Park and Fishman, 2011). This signal propagation is made possible through electrical coupling of the cardiac myocytes by gap junction channels. Each channel is composed of two hemi-channels, one from each participating cardiac cell, and in turn, these hemi-channels are made up of transmembrane proteins known as connexins (Van Veen *et al*., 2001). There are three main connexin isoforms expressed in the heart, namely connexin (Cx)-40, Cx43 and Cx45, each one displaying a distinct channel conductance, which is a major determinant of conduction velocity (Jansen *et al.*, 2010). Cx43 is by far the most abundantly expressed in the working myocardium and peripheral parts of the conduction system, whilst Cx45 is predominantly localised within the SA node.

A third and often overlooked aspect of cardiac autorrhythmicity is the extracellular milieu within which cardiomyocytes and other cardiac cells function. Even within the SA node, the pacemaker myocytes are enmeshed within a dense, fibrotic matrix, composed primarily of collagen, elastin, and fibroblasts (Csepe *et al.*, 2015). This “physiological fibrosis” plays a crucial role in the functioning of the heart’s pacemaker, in that it not only provides structural support, but also electrically insulates the SA node from the surrounding myocardium, preventing it from depressing the pacemaker action potential (Csepe *et al.*, 2015). SA node myocytes have also been shown to form functional gap junctions with fibroblasts via Cx43, which results in attenuation of spontaneous pacemaker activity (Fahrenbach *et al*., 2007).

Overall, the generation and maintenance of a normal cardiac rhythm relies on a pacemaker which can reliably produce rhythmical electrical activity, as well as intact conduction

pathways for the rapid propagation of this electrical impulse throughout the rest of the heart (Mangoni and Nargeot, 2008). Therefore, arrhythmogenesis comes down to an abnormality either in impulse formation, or a disturbance in impulse propagation (Antzelevitch and Burashnikov, 2011). There is, however, a great deal of overlap between these two basic mechanisms, especially given the important role of conduction even within the pacemaker tissue itself.

Diabetes is a risk-multiplier for disturbances in the normal cardiac rhythm, however the pathophysiological mechanisms remain obscure (Agarwal and Singh, 2017; Grisanti, 2018). Most of the experimental data available is derived from the adult diabetic heart. These studies have consistently shown that the cellular mechanisms involved in normal cardiac autorrhythmicity are adversely affected by hyperglycaemia (Ferdous *et al.*, 2016), and can therefore be used, in part, as the basis of understanding the developmental pathology of hearts exposed to hyperglycaemia *in utero*.

1.2.2 Impaired autorrhythmicity in the adult diabetic heart

Abnormalities of impulse formation are frequently encountered in diabetic patients, and epidemiological data on patients requiring pacemaker replacement for severe bradycardia have revealed an overrepresentation of individuals with type 2 diabetes (Podlaha and Falk, 1992). Animal models of diabetes mellitus have been indispensable to the study of pacemaker dysfunction, and in these studies, diabetes is almost invariably associated with a gradual decline in baseline heart rate (Soltysinska *et al.*, 2014). This bradycardia is not only observed *in vivo*, but in spontaneously beating, isolated perfused hearts as well, where the heart rate is determined solely by pacemaker activity and is independent of autonomic regulation (Huang *et al.*, 2017). Several attempts have been made to determine the molecular mechanisms underlying this intrinsic bradycardia in the diabetic heart. Two recent studies by Howarth *et al* and Ferdous *et al* revealed significant differences in the mRNA profiles of diabetic SA node when compared to controls (Ferdous *et al*., 2016; Howarth *et al*., 2018). Of particular interest is that there was a significant downregulation of HCN4, which is the dominant HCN channel isoform responsible for mediating the pacemaker current (I_f). This is in keeping with an earlier study by Huang *et al*, which showed a 70% reduction in

HCN2 and a 58% reduction in HCN4 mRNA expression in the diabetic SA node (Huang *et al.*, 2017). It is reasonable to expect that a reduced expression of these HCN channels would lead to a slowing of cardiac pacemaker activity, and thus contribute to the intrinsic bradycardia observed in diabetes. Several studies have also shown a reduced I_f current density (Kennedy *et al*., 1993), and while this may be the result of reduced channel expression, impairment in HCN channel modulation have been suggested to play a role. Zhang *et al* recently showed a significant downregulation of β-adrenergic receptors in the SA node of diabetic rats. This would correspond with a decrease in intracellular cAMP, which is the primary modulator of I_f (Zhang *et al.*, 2019). The exact molecular pathways involved in downregulating HCN channels and reducing I_f current density in diabetes remain unknown, although it is thought that oxidative stress may be the key underlying trigger.

Abnormal conduction is a common mechanism underlying cardiac arrhythmias, and it is the result of mechanical and electrophysiological heterogeneity within the myocardium (Tse *et al.*, 2016). This heterogeneity lends itself to a phenomenon known as *re-entry*, in which an electrical impulse no longer follows the normal circuit, but rather rapidly and continuously circulates around an obstacle, looping back upon itself. The obstacle can be an anatomical one, such as an area fibrotic tissue, or it can be a functional one such as a small region of the heart with different electrophysiological properties (Gaztañaga *et al*., 2012). The diabetic heart is a substrate for abnormal propagation of the cardiac impulse, and animal studies have provided some useful mechanistic insights into the pathophysiology of these conduction defects. A prolonged sinoatrial conduction time is a common finding in experimental studies of the diabetic heart (Senges *et al.*, 1980). The conduction velocity is largely determined by the spread of ionic currents via gap junctions, between electrically coupled myocytes. Howarth *et al* recently showed that the expression of gap junction proteins Cx43 and Cx45 were both downregulated in the diabetic rat SA node when compared to controls (Howarth *et al.*, 2018b). These findings are in keeping with those of a more recent study, in which all three connexin isoforms were significantly downregulated in the cardiac conduction system of diabetic rats, including the pacemaker (Zhang *et al.*, 2019). This downregulation would result in impaired electrical communication between adjacent cardiomyocytes, explaining the conduction delay so often observed in electrophysiological studies of the diabetic SA node. Interestingly, two earlier studies using a different animal

model of diabetes, showed an *upregulation* of Cx45 in the diabetic SA node (Howarth *et al.*, 2007; Ferdous *et al.*, 2016). Because Cx45 has a lower unitary conductance compared to the other gap junction channels, its increased expression might explain the reduced conduction velocity in the SA node of these diabetic rats (Tse *et al.*, 2016). A major limitation of these studies is that many of them do not analyze the subcellular distribution of these gap junction proteins within the cardiac pacemaker. In fact, the heart has a very large conduction reserve, which means that even drastic reductions in the expression of connexin proteins may only have a modest impact on cardiac conduction (Jansen *et al.*, 2010).

In addition to structural and functional remodelling of gap junction channels, cardiac fibrosis has been shown to be a key promoter of conduction abnormalities in the diabetic heart (Liu *et al.*, 2012). It does so by physically disrupting the electrical coupling between cardiomyocytes, and therefore slowing down impulse propagation through the conduction system. With regards to its pathogenesis, transforming growth factor (TGF)- β1 is considered the main pro-fibrotic cytokine in the heart, and it is secreted by various cell-types, including macrophages, fibroblasts, and cardiomyocytes themselves (Jia *et al.*, 2020). TGF-β1 activation results in phosphorylation of downstream signaling molecules called Smads, of which Smad3 is the most heavily implicated in cardiac fibrosis. This TGF-β1/Smad3 cascade ultimately leads to activation of fibroblasts into myofibroblasts, and increased collagen deposition within the extracellular matrix. In the diabetic heart, inflammation, oxidative stress, and advanced glycation end products are all potent stimulators of this TGF-β-mediated fibrosis (Singh *et al.*, 2008; Jia *et al.*, 2020). Even in whole mouse embryos that were exposed to high glucose culture medium *in vitro*, hyperglycaemia was shown to upregulates TGF-β1 expression, along with the expression of various extracellular matrix proteins (Smoak, 2004).

Taken together, these findings from experimental models of diabetes provide compelling evidence of altered electrophysiology and a propensity to arrhythmogenesis in the diabetic heart. The findings, however, cannot be extrapolated to the embryonic heart exposed to hyperglycaemia *in utero*. This is because with cardiomyocyte maturation, there is withdrawal from the cell cycle, with cardiomyocytes becoming terminally differentiated and losing their proliferative capacity (Nakano *et al*., 2021). Therefore, in the adult heart, most disease states

are accompanied by cardiac hypertrophy and scar formation, a process known as pathological remodelling (Lázár *et al*., 2017). That being said, there are some striking similarities between cardiomyocytes isolated from adult rats in heart failure, and those from developing, neonatal rats (Lipsett *et al.*, 2019). It is now well established that during periods of metabolic or haemodynamic stress, such as ischaemia, pressure overload or arrhythmia, all of which occur more frequently in diabetics, there is extensive remodelling of the cardiac phenotype and a compensatory reactivation of immature, foetal cardiac genes (Rajabi *et al.*, 2007). For instance, in the developing heart, HCN channels are expressed abundantly in the ventricles, a phenomenon which is often referred to as diffuse automaticity. With maturity, HCN expression becomes restricted to the cardiac conduction system (Choudhury *et al*., 2015). In pathological states such as heart failure and diabetic cardiomyopathy, there is re-expression of I_f/HCN within the ventricles, and this is thought to be an important contributor to the formation of malignant arrhythmias in this patient group (Kuwabara *et al.*, 2013). Therefore, by understanding how embryonic cardiomyocytes respond to the stress of hyperglycaemia *in utero*, we may even provide useful insights into why the compensatory reversion to an immature cardiac phenotype quickly becomes maladaptive and dysfunctional in the adult diabetic heart.

1.2.3 Impaired autorrhythmicity in the foetal heart during diabetes

1.2.3.1 How the foetal heart differs from the adult heart

To better understand the effect of hyperglycaemia on the autorrhythmicity of the developing heart, it is worth highlighting some key differences between the mature adult heart and the foetal heart *in utero*. The foetal heart is geared towards surviving in a relatively hypoxic, low-oxygen intrauterine environment (Rajabi *et al*., 2007). To this end, there are numerous structural, biochemical, and electrophysiological adaptative mechanisms in place, which make the embryonic heart different from the neonatal heart, and even more so from the adult heart. For instance, whilst adult cardiomyocytes rely heavily on fatty acid oxidation as their primary fuel source, the foetal heart metabolism relies on carbohydrates, which are a far more energy efficient substrate (Tan and Lewandowski, 2020). Another unique feature of the embryonic heart is its capacity for *de*

novo cardiomyocyte synthesis. In the postnatal period, heart growth occurs primarily by an increase in cardiomyocyte size rather than number, although some regenerative capacity has been demonstrated shortly after birth (Porrello *et al.*, 2011).

Animal studies have provided useful insights into the development of the cardiac conduction system in the embryo, however the exact molecular pathways involved remain unclear (Jongbloed *et al.*, 2004). Electrocardiograph (ECG)-like recordings have been obtained even at very early stages of cardiac development, indicating the presence of a functional conduction system in the embryonic heart tube (Kornblum *et al.*, 2013). This early stage is characterised by the presence of slow impulse propagation resulting in a peristaltic-like contraction of the developing heart tube. Moreover, the action potentials recorded during this phase display slow spontaneous depolarizations typical of SA nodal cells, which is in keeping with the concept of diffuse automaticity in the immature heart (Watanabe *et al.*, 2016). Importantly, HCN4 expression in the mouse embryo has been shown to be very dynamic (Liang *et al*., 2015). Initially it is expressed throughout the developing heart tube, but by embryonic day 16, it is found to be more restricted to the conduction system. Whether these findings hold true for the human embryonic heart remains unclear. The pattern of cardiac connexin expression on the other hand, has been shown to be quite similar between the mouse and human foetal heart, with connexin 43 being robustly expressed within the working myocardium, and connexins 40 and 45 being confined to the cardiac conduction system (Coppen *et al.*, 2003). As the heart matures, a second and faster pattern of conduction emerges within the atria and ventricles (Moorman *et al.*, 1998), and an adult-type ECG tracing can be seen, indicating sequential activation of these heart chambers (Paff *et al*., 1968).

1.2.3.2 Clinical evidence of arrhythmias in infants of diabetic mothers

It is well established that both pre-existing and gestational diabetes mellitus are major risk factors for foetal cardiac pathology (Al-Biltagi *et al*., 2021). Although most cardiac changes in infants of diabetic mothers are transient and resolve spontaneously during the postnatal period, a recent retrospective cohort study on children born to poorly controlled diabetic mothers showed that certain cardiac and vascular changes do persist until much later in the

offspring's life (Hoodbhoy *et al.*, 2019). Maternal diabetes has been shown to produce pathological heart rates, including bradycardia, in infants of diabetic mothers (Shankar *et al.*, 2019). These heart rhythm disturbances are generally under-reported in the literature, perhaps because they are not as readily detectable as the structural defects. One study found that atrial tachyarrhythmias are more common in infants of diabetic mothers, even in the absence of structural cardiac abnormalities (Pike *et al.*, 2013). In a study by Yli *et al.*, foetal ECG recordings during labour revealed that ST segment changes were more prevalent in offspring of diabetic mothers, independent of intrapartum hypoxia (Yli *et al.*, 2008). This finding was thought to reflect an impaired ability of the myocardium to adapt to stress, a vulnerability which may well express itself later in life, in response to various insults and environmental exposures. In yet another study, ECG analysis revealed a prolonged QT dispersion among neonates of diabetic mothers, a phenomenon which has been linked to increased risk of malignant arrhythmias and sudden death (Arslan *et al.*, 2014).

The mechanisms underlying these electrophysiological aberrations in offspring of diabetic mothers are poorly understood and most likely involve a complex interplay between factors such as foetal hyperglycaemia, reflex hyperinsulinemia, oxidative stress, inflammation, and foetal hypoxia (Hoodbhoy *et al.*, 2019). Of all these sequelae of maternal diabetes, however, hyperglycaemia has been identified as the key teratogen in all diabetic pregnancies (Nakano *et al*., 2021), with strict maternal glucose control being the single most effective intervention in lowering risk of cardiac complications in infants of diabetic mothers (Al-Biltagi *et al*., 2021). Additionally, animal models of gestational diabetes have shown that with an increase in maternal plasma glucose levels, there is a proportional rise in foetal glucose levels (Singh *et al*., 1997). Very little is understood about the impact of hyperglycaemia on cardiomyocyte development as seen in a diabetic pregnancy, particularly as it pertains to electrophysiological remodelling and arrhythmogenesis. The study of foetal electrophysiology, which has mainly been carried out in animals, is fraught with challenges, such as the small size and fragility of the cardiac tissue, as well as the rapidly changing topology of the heart as it grows (Watanabe *et al.*, 2016).

1.2.3.3 Foetal arrhythmogenic mechanisms in diabetes

Disturbed foetal glucose metabolism secondary to maternal hyperglycaemia is thought to play a critical role in the structural cardiac defects so frequently observed in offspring of diabetic patients (Nakano *et al*., 2021). Exposure of the foetal heart to hyperglycaemia has been shown to cause dysregulation of signalling pathways which are critical to cardiac development. These include the Notch, Wnt and TGF-β signalling pathways. Moreover, hyperglycaemia-induced oxidative stress has also been shown to impair migration of neural crest cells into the heart, resulting in defects of the outflow tract (Morgan *et al.*, 2008). Given that these neural crest cells also contribute to the formation of the cardiac conduction system (Nakamura *et al*., 2006), it is possible that exposure of the foetal heart to hyperglycaemia during early cardiogenesis causes abnormalities of the electrical signalling pathways, however this is an area of research that remains largely unexplored. In fact, research on foetal cardiac remodelling has largely been focused on structural changes, such as cardiac defects and malformations (Crispi *et al.*, 2020). Even though it has been shown that changes to the cardiac conduction system of the developing heart can result in life-threatening arrhythmias (Jongbloed *et al.*, 2004), the role of hyperglycaemia in foetal arrhythmogenesis is unknown. It has previously been shown that stem cell-derived cardiomyocytes exposed to hyperglycaemia *in vitro* display delayed cardiac maturation and supressed expression of cardiac transcription key factors such as NKX2.5 and TBX5 (Yang *et al.*, 2016; Nakano *et al.*, 2017). The effect of hyperglycaemia on the beating profile of these immature cardiomyocytes, however, remains unexplored.

Chapter 2: Purpose of the present study

2.1 Problem statement

Hyperglycaemia is a major risk factor for malignant cardiac dysrhythmias, especially in the offspring of poorly controlled diabetic mothers. The effect of hyperglycaemia on the cardiac conduction system of the developing heart, however, is poorly understood, with most studies being conducted in the adult diabetic heart.

2.2 Aim of the study

The aim of the present study is to explore the effects of hyperglycaemia on the autorrhythmicity and impulse propagation in a foetal heart model of spontaneously beating mouse embryonic stem cell (mESC)-derived cardiomyocytes.

2.3 Specific Objectives

1. To differentiate pluripotent mESCs into spontaneously pulsatile cardiomyocytes through embryoid body (EB) formation.
2. To characterise the effect of high glucose on the autorrhythmicity, pacemaker channel modulation, and responses to arrhythmogenic drugs of mESC-derived cardiomyocytes.
3. To assess the impact of high glucose on the intercellular propagation of the cardiac impulses.
4. To explore possible molecular mechanisms underlying foetal cardiac remodelling in diabetes, with a specific focus on the TGF-β canonical pathway.

2.4. Significance of the present study

The prevalence of diabetes mellitus and the burden of its cardiovascular complications is increasing worldwide (Pheiffer *et al.*, 2018). As such, the need for targeted therapeutic interventions has never been greater, particularly in the offspring of diabetic mothers, who face the lifelong and potentially life-threatening cardiac sequelae of uncontrolled

hyperglycaemia. The purpose of this present study is to provide novel insights into foetal cardiac remodelling under hyperglycaemic conditions, with a specific focus on the cardiac conduction system and the pathophysiology of malignant arrhythmias. Moreover, by providing a better understanding of how diabetes impacts on the developing embryonic heart, this study may potentially provide insights into the pathological remodelling of the adult diabetic heart, whose primary response to chronic hyperglycaemia is to re-activate the foetal cardiac gene programme.

***

Chapter 3: Methods and Materials

3.1 Stem Cell Culture and Proliferation

Undifferentiated mESCs of the OLA 129 cell line (a gift from Professor Brombacher at the University of Cape Town) were used in this study and the pluripotency of these cells has previously been verified by Aboalgasm *et al*. (Aboalgasm *et al*., 2021). The mESCs were plated onto a feeder layer of mitomycin-inactivated mouse embryonic fibroblasts (iMEFs) and incubated for a period of 3 days, under standardised cell culture conditions (5% humidified CO_2 and 37°C). The iMEF feeder layer supports the growth of the stem cells and helps to maintain their pluripotency by secreting nutrients and growth factors into the culture medium. Unless otherwise stated, all cell culture chemicals were purchased from Thermo-Fisher Scientific (LTC Tech, SA). To prepare the feeder layers, culture dishes were gelatinised with 0.1% gelatine and incubated for 1 hour at 37°C. The iMEFs were then collected from the liquid nitrogen storage facility, where they were frozen in MEF culture medium composed of 87.9% Dulbecco's Modified Eagles Medium (DMEM), 10% foetal bovine serum (FBS), 1% Glutamax, 1% penicillin/ streptomycin and 0.1% β-mercaptoethanol. Dimethyl sulfide (DMSO), a commonly used cryoprotectant, was added at a concentration of 10% to ensure the health and viability of the iMEFs post-freezing, however DMSO is toxic to living cells at these this concentration and so the iMEFs were thawed quickly in a waterbath and added to 4mL of fresh MEF culture medium to minimises DMSO toxicity. This thawing step was followed by a 5-minute centrifugation at 1 500 relative centrifugal force (rcf), before discarding the supernatant and resuspending the iMEF pellet in 1mL of MEF medium. This cell suspension was then added to the gelatinised culture dishes and incubated for 48hours to allow adequate time for the iMEFs to adhere to the dish.

Approximately 2 hours prior to plating the mESCs onto the feeder layers, the MEF culture medium was exchanged for stem cell (ES) medium, which contains DMEM, 15% foetal bovine serum, 1% glutamax, 1% penicillin/ streptomycin, 0.1% β-mercaptoethanol and 1:200 leukaemia inhibitory factor (LIF, catalog # A35935, Thermo Fisher). The addition of LIF to the

ES medium is particularly important, as it works synergistically with the iMEF feeder layer to maintain the mESCs in their undifferentiated state (Humphrey, 2004). The mESCs were collected from liquid nitrogen storage, thawed and centrifuged as described above for iMEFs. After discarding the supernatant, the pellet was resuspended in 1 mL of ES medium and the mESC cell suspension was added to the feeder layer. The mESCs were then incubated at 37°C for a period of 3 to 4 days to allow them to proliferate, with the ES medium being refreshed after 2 days. The growth of the merging mESC colonies was monitored daily using the EVOS microscope (EVOS XL Core, Invitrogen). After 3 to 4 days, when the stem cell colonies had reached a confluency of ± 75% (i.e., 75% of the culture dish surface was covered by stem cells), the mESCs were then passaged and plated onto newly prepared feeder layers. This passaging or subculturing step is important, as it prevents 'overcrowding' of stem cell colonies and facilitates their expansion.

The passaging step was carried out by first aspirating the ES media from the culture dishes and enzymatically dissociating the stem cells from the feeder layers by adding 5mg/mL of Dispase V solution, followed by a 15-to-20-minute incubation period at 37°C. The dispase enzymatic activity was then inactivated by adding MEF medium to the culture dish. The mESCs were transferred to a 15mL Falcon tube and centrifuged for 5 minutes at 1500 rcf, before being resuspended in 1mL of ES medium and plated onto the new feeders as previously described. This was followed by a 48-hour incubation at 37°C allow stem cell proliferation, before proceeding to the differentiation step. To exclude contamination by mycoplasma bacteria, which are resistant to most antibiotics, mESCs were stained with the Hoechst nuclear dye and visualised under fluorescent microscopy (EVOS™ M5000, Thermo Fisher Scientific; *see appendix* **Fig. A1**).

3.2 Stem Cell Cardiac Differentiation

The differentiation of pluripotent mESCs into cardiomyocyte-like stem cells was carried out using the validated hanging drop protocol adapted from Wang and Yang (Wang and Yang, 2008). Hanging drop culture provides an optimal environment for mESCs to differentiate into three-dimensional aggregates called embryoid bodies (EBs). Each EB yields cells of different lineages, including cardiac, as evidenced by the onset of spontaneous contractile activity

within 7 days of differentiation. The first day of hanging drop was considered Day 0 of the mESC differentiation process. Briefly, mESC colonies were dissociated from the iMEF feeders and centrifuged as described above in the passaging step. The mESC pellet was resuspended in 1mL of differentiation medium (87.9% DMEM, 10% FBS, 1% Glutamax, 1% penicillin/ streptomycin and 0.1% β-Mercaptoethanol) containing baseline glucose concentration of 25 mM, which is considered standard in stem cell culture protocols (Wang and Yang, 2008). After thorough trituration to form a single cell suspension, the cells were counted using a counting chamber haemocytometer. The cell suspension was adjusted to achieve a concentration of 1000 cells per 20μL of ES media. This step is critical, as it minimises the heterogeneity of the EBs by ensuring a fixed number of mESCs in each hanging drop. Moreover, EBs with a starting number of 1000 mESCs have been shown to have the highest degree of cardiac differentiation compared to lower and higher cell concentrations(Chen *et al.*, 2011). Hanging droplets were made by forming rows of 20μL drops of the cell suspension on the inner surface of a 10cm tissue culture dish (*see appendix*, **Fig. B1 and B2**). The lid was carefully inverted onto the culture dish, which contained 10mL of PBS to prevent evaporation of medium from the hanging droplets. The culture dish was incubated and left undisturbed for 2 days under standard culture conditions. With the help of gravity, mESCs aggregate at the bottom of the hanging drops, triggering specific cell-cell interactions, which are mediated by transmembrane adhesion molecules known as cadherins (Zeevaert *et al.*, 2020). These cell-cell interactions activate key developmental signalling pathways which guide cellular differentiation and growth, a process which very similar to early embryogenesis.

On Day 3 of differentiation, the hanging drops containing EBs were transferred into non-adherent bacteriological dishes containing 10mL of differentiation medium, and incubated for 4 days at 37°C. This period of suspension culture prevents stem cell attachment to the culture dish and other substrates, and instead promotes continued spontaneous aggregation of mESCs into EBs. The differentiation medium in the bacteriological dishes was refreshed after 2 days, by aspirating 5mL of the old medium and adding 5mL of new medium. On Day 7, EBs were transferred from suspension to adherent culture. Briefly, 12-well plates with or without coverslips were gelatinised with 0.1% gelatine and incubated for 30 minutes under standard conditions. After aspirating the excess gelatine, 1mL of differentiation medium was

added to each well. EBs were then picked up one-by-one using a pipette, and transferred into the 12-well plate. Care was taken to ensure that each well was occupied by only one EB, to avoid the unknown effects of EB-to-EB interaction on functional characteristics.

The EBs were incubated under standard cell culture conditions and monitored daily for morphological changes and onset of spontaneous beating activity, a marker of cardiac differentiation, using an EVOS XL Core light microscope. EBs were considered mature between Days 17 to 21 post cardiac differentiation, and all imaging and characterization of EB pulsatile activity was carried out during this period. The unit of measurement in this study was defined as a single EB, and in instances where an EB contained two or more distinct beating areas, the larger or more robust beating foci was included in analysis. All EBs were included in analysis, provided there had been no evidence of infection or Mycoplasma contamination throughout the entire culture process. Signs of contamination include poor EB growth, as well as changes in the colour and smell of culture medium.

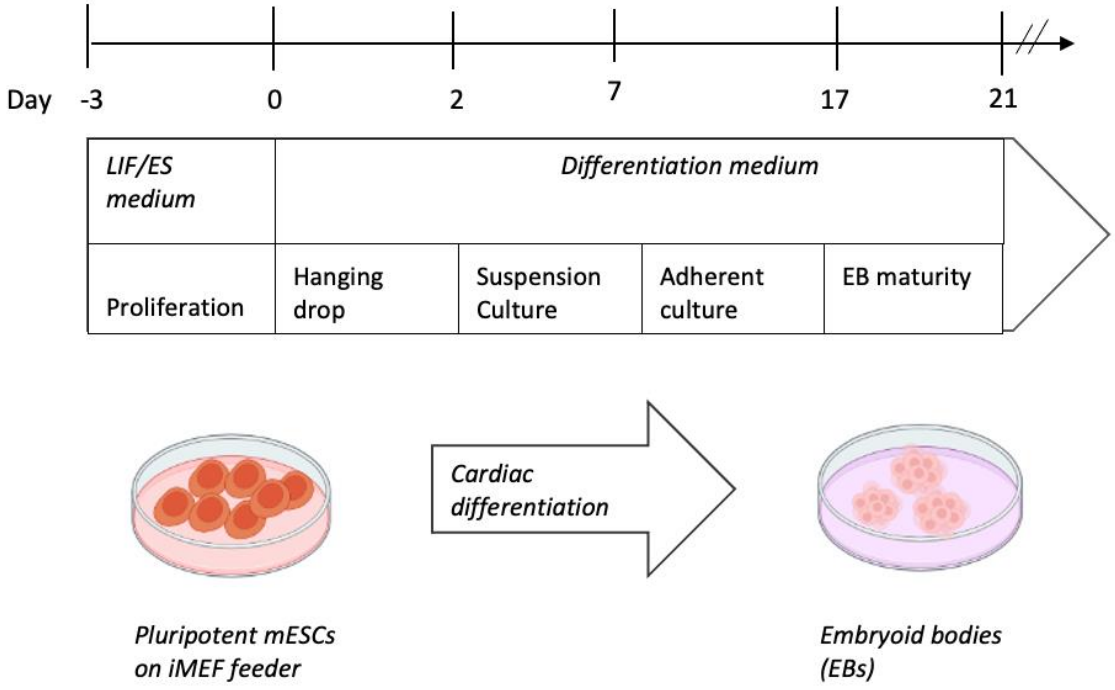

Fig 1. Schematic diagram of cardiac differentiation protocol. Pluripotent mouse embryonic stem cells (mESCs) were grown and proliferated on inactivated mouse embryonic fibroblast (iMEF) feeder layers over a period of about 3 days, in embryonic stem cell (ES) medium containing leukaemia inhibitory factor (LIF). On Day 0, which was considered to be the first day of the cardiac differentiation protocol, embryoid body (EB) formation was carried out using the hanging drop method in differentiation medium. EBs were transferred to suspension culture on Day 2, then adherent culture from Day 7 onwards. EBs were considered mature between Day 17 and 21. *Images created using the BioRender software (BioRender.com)*

3.3 Experimental design and interventions

To mimic hyperglycaemia, the pathological hallmark of diabetes, a second experimental group was introduced, in which EBs were grown under high glucose conditions of 50 mM from Day 0 of the differentiation protocol. Given that the default glucose concentration in stem cell culture is supraphysiological to begin with (i.e., 25 mM), this exaggerated hyperglycaemia only represents a doubling of the baseline glucose conditions, a change similar to that found in real diabetic patients. Moreover, a 50 mM glucose concentration has been used as a hyperglycaemia model in previous *in vitro* cardiac studies (Ali *et al.*, 2004; Aboalgasm *et al.*, 2021). Given that even in the clinical setting, hyperglycaemia is invariably accompanied by uncorrected hyperosmolarity (Stoner, 2017), this study, and several other cardiac *in vitro* studies (Han *et al.*, 2015; Aboalgasm *et al.*, 2021), did not include an osmotic control group.

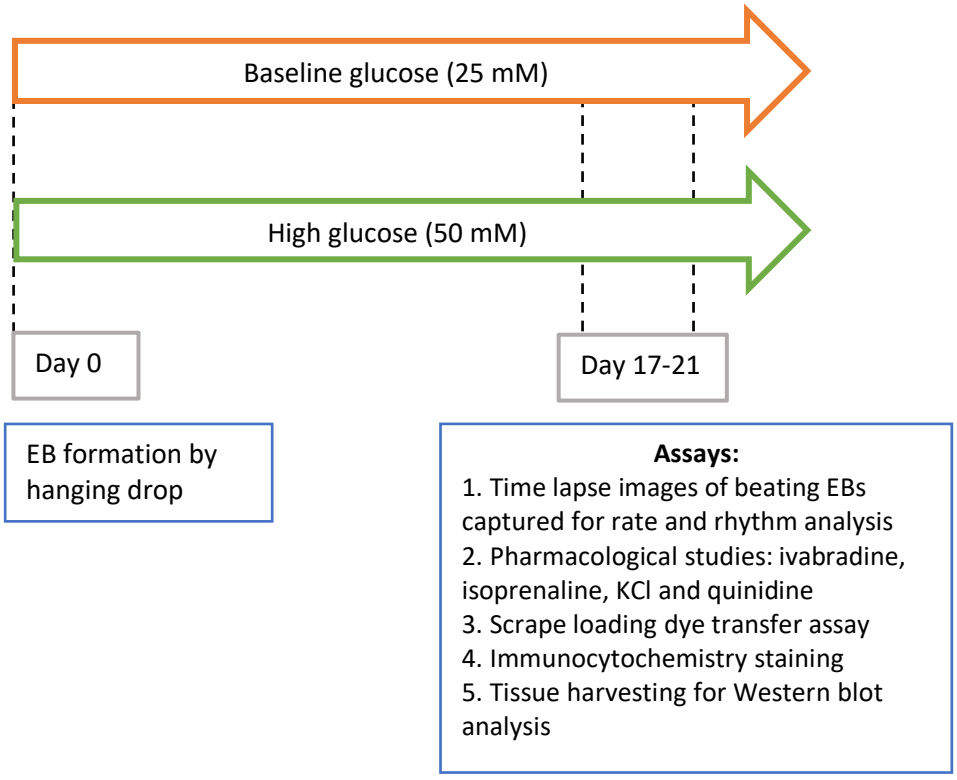

Fig 2. Schematic diagram of experimental design. On Day 0, pluripotent mESCs were differentiated into embryoid bodies (EBs), in differentiation medium containing either baseline (25 mM) or high (50 mM) glucose concentrations. At Day 17-21, time lapse images of mature, beating EBs were taken for rate and rhythm analysis. EBs were stimulated with various pro-arrhythmogenic drugs, and their beating response reordered. The scrape loading dye transfer assay and harvesting of tissue for western blot analysis were also carried out during this period.

Baseline rate and rhythm analysis

Time lapse images of beating EBs at Day 17 to 21 were captured on the EVOS™ M5000 imaging system (Thermo Fisher Scientific). The images were analysed using ImageJ software (ImageJ, NIH) coupled with the motion-detecting macro Myocyter™ (Grune *et al.*, 2019). This macro detects and quantifies cardiac or cellular contractions, providing graphical output in the form of amplitude of contraction over time (see **Fig. 4a** in *Results* and **Fig. C1** in *Appendix*). From this output, the beating rate and variations in beat-to-beat intervals were determined, and episodes of ectopic beats detected.

Stimulation with pharmacological agents

To assess whether hyperglycaemia modulates pacemaker response to ß-adrenergic stimulation, beating EBs were recorded 2 minutes before and 2 minutes after stimulation with isoprenaline (Sigma, SA; catalog # 15672) 12 μM, dissolved in distilled water *(see Appendix*, **Fig. C2**). The sensitivity to isoprenaline was calculated as the percentage (%) increase in beating rate from pre- to post-stimulation. Pacemaker sensitivity to ivabradine (Sigma, SA, catalog # SML0281), a hyperpolarization-activated, cyclic nucleotide-gated (HCN) channel blocker was explored. Following application of ivabradine (10 μM; dissolved in distilled water), EBs were recorded as described in **Fig. C2** *(see Appendix).*

To test the sensitivity of cells to pro-arrhythmogenic stimulation, the EBs were stimulated with the following arrhythmogenic drugs: potassium chloride (KCl; Sigma, SA; catalog # P9333) 12.5 mM dissolved in distilled water, isoprenaline 12 μM in distilled water, and quinidine (Sigma, SA; catalog # Q3625) 1 μM dissolved in DMSO. Time lapse images were recorded as for KCl, and the occurrence of ectopic beats noted. For quinidine, which predominantly blocks voltage-gated Na^+ and K^+ channels, and causes cessation of beating activity, EBs were recorded at 2-minute intervals following drug application (*see Appendix*, **Fig. C2**)**,** and the time interval during which onset of asystole occurred, was documented.

Western blot analysis

Western blot analysis was performed on tissue samples prepared from mature functional EBs (day 17-21). To harvest the tissues, 8 to 10 beating EBs were selected from each experimental group (control vs high glucose) and the culture medium aspirated from their respective wells. A few drops of radioimmunoprecipitation assay (RIPA) lysis buffer (50 mM Tris-HCl, 150 mM NaCl, 1% Triton X-100, 0.5% sodium deoxycholate, 0.1% sodium dodecyl sulphate (SDS), pH 7.4) with 1% protease and phosphatase inhibitor cocktail was added to each well. The RIPA buffer facilitates the extraction of membrane and cytoplasmic proteins though total cell lysis and protein solubilization, and the inhibitor cocktail is critical for protein preservation (Janes, 2015)

Next, the EBs were gently scraped off the bottom of the wells with a syringe plunger and transferred to an Eppendorf tube, which was left on a roller for 30 minutes. This is to allow sufficient time for the tissue sample to mix with the RIPA buffer, causing cell lysis and release of proteins. The cell lysates were then centrifuged at 15000 relative centrifugal force for 30 minutes at 4°C (Labnet International, NJ07095, USA), and the supernatant collected and kept on ice to minimise protein degradation. The protein concentration of each sample was determined using the Pierce protein assay kit (Thermo Scientific, Rockford, USA). This kit contains several vials of bovine serum albumin at a fixed concentration of 2 mg/mL. A series of dilutions of known concentration were prepared, and their absorbance measured using a spectrophotometer (see full protocol in *Appendix*). From this, a standard curve was constructed, against which the protein concentration of each of the samples could be quantified (see **Fig. C3a** in *Appendix*). The samples were then adjusted to a final protein concentration of 30μg/20μL by diluting with RIPA buffer (preliminary experiments showed that this concentration of protein was sufficient to obtain a good signal). This step is critical, as it ensures that an equal amount of protein from each sample is introduced into the sodium dodecyl sulfate (SDS)-polyacrylamide gel electrophoresis (PAGE) step. SDS-PAGE is a technique used to separate proteins based solely on their molecular weight. First, 10% SDS-polyacrylamide gels were prepared using the TGX FastCast™ acrylamide kit from Bio-Rad, SA (catlalog # 1610173; see **Fig. C3b** in *Appendix*). Then, 20μL of each sample was loaded onto the gel, alongside a prestained protein ladder (Thermo Fisher, catalog # 26616).

Electrophoresis was carried out for 30 minutes at 150 V, using the Mini-Protean Tetra Cell system (Bio-Rad, SA; catalog # 1658002). To confirm the presence of protein bands in the gel and therefore successful electrophoresis, gels were soaked in Coomassie Brilliant blue dye (Bio-Rad, SA; catalog # 161-0436), and the excess stain removed with 30% methanol (see **Fig. C3d** and full western blot protocol in *Appendix*). Unfortunately, once stained with this dye, the gels can no longer be used for the next step, which is protein transfer. Therefore, the Coomassie staining was only used during the initial troubleshooting stages of the protocol.

Following successful electrophoresis, the protein in the gel was transferred to a polyvinylidene fluoride (PVDF) membrane which was pre-soaked in methanol for 1 minute to activate it. The protein transfer was carried out using a semi-dry transfer unit (Tran-Blot Turbo Transfer System, Bio-Rad, SA) and pre-mixed transfer buffer (Bio-Rad, SA; catalog # 1610734). Ponceau staining was used to confirm successful protein transfer. This Ponceau dye (Sigma, catalog # D4540) binds reversibly to any proteins present on the membrane and appears as pink bands once excess stain has been rinsed off (see **Fig. C3e** in *Appendix*). The membrane was then blocked for 1 hour at room temperature with 3% non-fat milk in phosphate buffered saline with 0.1% Tween-20 (PBS-T) to prevent nonspecific binding of antibodies and reduce background noise. In cases where a phosphorylated antibody was being used (e.g., phosphor-Smad3), 3% BSA in PBS-T was used instead of milk, to avoid unwanted interactions with milk proteins such as casein, which is a phosphoprotein itself (Yang and Mahmood, 2012). The membrane was incubated overnight at 4°C in primary antibody (unless otherwise stated, all from Thermo-Fisher Scientific) directed against one of the following proteins of interest: connexin-43 (cx-43, 1:1000; catalog # 35-5000), transforming growth factor beta (TGF-β, 1:1000; MA5-16949) and hyperpolarization-activated, cyclic nucleotide-gated (HCN) channel 4 (HCN 4, 1:500; MA3-903). Beta actin (1:5000; MA5-15739) and alpha-tubulin (1:2000, Sigma-Aldrich; catalog # T8203) were used as the housekeeping controls. All antibodies were diluted in either 3% non-fat milk or 3% BSA in PBS-T. Next, the membrane was washed with PBS-T for 20 minutes and incubated with horseradish peroxidase (HRP)-conjugated secondary antibody (Goat anti-mouse IgG, Thermo-Fisher Scientific; catalog # SA5-10276) for 2 hours at room temperature. The membrane was washed again with PBS-T to remove excess antibody, then incubated with enhanced chemiluminescence (ECL) detection solution (Clarity Western ECL substrate, Bio-

Rad SA; catalog # 1705061) for 3 minutes. ECL is a highly sensitive method for detecting proteins which are bound to the membrane. The HRP enzyme which is conjugated to the secondary antibody reacts with substrates such as luminol in the ECL solution, releasing a light signal (Mruk and Cheng, 2011). This signal was captured by exposing the membrane to x-ray film (Agfar Healthcare, SA) in a darkroom. The x-ray film was scanned, and the images were analysed using ImageJ software (Image J, NIH Image).

Scrape loading/dye transfer assay

The scrape loading/dye transfer assay using lucifer yellow (LY) was used as a functional means to assess gap junctional intercellular communication (GJIC) within the EBs. The protocol used in this study was adapted from Babica *et al* (Babica *et al*., 2016). Briefly, Day 17 to 21 EBs grown on glass coverslips were selected and rinsed gently with phosphate buffered saline (PBS) containing calcium and magnesium (CaMg-PBS). The addition of calcium and magnesium to the PBS helps to maintain cell adhesion and prevent EBs from lifting off the coverslips. Each EB was transferred (on its coverslip) to a 35 mm petri dish, and 1 mL of LY dye solution (1mg/mL in distilled water, Sigma, SA) was added to cover the EBs. A curved surgical scalpel blade was used to make three clean cuts across each EB (**Fig. C4**, in *Appendix*) and the dish was incubated for 5 minutes at room temperature, under a foil cover to minimise light exposure and photobleaching of the dye. This incubation period allows sufficient time for the LY dye to be taken up by the cells whose membranes were physically disrupted by the scraping, then transferred to adjacent cells by way of functional gap junction channels. The dye solution was then aspirated from the dish and the EBs rinsed gently with CaMg-PBS to remove excess dye. The EBs were fixed by adding a few drops of 10% formalin solution. This was followed by immediate visualisation using the EVOS™ M5000 inverted epifluorescence microscope in the green fluorescence channel (Thermo-Fisher Scientific). Images were obtained, and the distance of dye transfer was measured at several points along the scrape line using ImageJ software (ImageJ, NIH). The average dye transfer distance was calculated for each EB, and this represented the overall extent of LY-dye spread.

Immunocytochemistry

Immunocytochemistry was performed to analyse the expression patterns of cardiac sarcomeric protein α-actinin 2, and the major cardiac gap junction connexin-43. Mature EBs (day 17-21) plated on glass coverslips were rinsed briefly with phosphate-buffered saline (PBS), then fixed with 4% paraformaldehyde, permeabilized with ice-cold methanol, and blocked using 3% bovine serum albumin (BSA) with 0.01% Triton X-100 in PBS. Samples were incubated overnight (at 4 ^{o}C in PBS with 1% BSA) with primary antibodies against α-actinin 2 (1:250; #701914, Thermo Fisher Scientific), connexin 43 (1:200; Thermo Fisher Scientific). The samples were then incubated with Alexa Fluor 488- (dilution 1:5000, #715-546-150, Amersham) or Cy3- (dilution 1:1000; #711-166-152, Amersham) conjugated secondary antibodies for 2 hours at room temperature. The samples were counterstained with the nuclear stain Hoechst 33258 (0.5 µg/ml; Sigma, SA) and imaged on a Zeiss LSM880 confocal microscope (Zeiss.com; under 40x magnification) using ZEN software (Zeiss.com). Images were analysed using ImageJ (NIH, USA).

Statistical analysis

Data Presentation

The data in this study were presented as box plots, which provide a clear distribution of observations within each group. Descriptive statistics, including means, were also calculated to summarize the central tendency of the data. The value *n* was used to denote the number of embryoid bodies (EBs) studied in each experimental group, providing transparency about the sample size.

Statistical methods

All statistical analyses were conducted using Statistica (version 13) software to assess the differences between groups. The choice of statistical tests was guided by the nature of the data and its adherence to normality assumptions.

Normality Assessment: Prior to conducting hypothesis tests, normality of the data was assessed using the Shapiro-Wilk test. This test was applied to evaluate whether the data in each group followed a normal distribution. In cases where the data were found to be non-normally distributed, alternative non-parametric tests were employed.

Parametric Data: For data that met the assumption of normality, specifically parametric data, an unpaired t-test was utilized. The unpaired t-test is appropriate for comparing means between two groups when the data follow a normal distribution. The significance threshold for this test was set at a p-value of ≤ 0.05, indicating statistical significance.

Non-Normally Distributed Data: In instances where the data did not conform to the normal distribution assumption, such as the case of "time to asystole post-quinidine stimulation," a Mann-Whitney U test was employed. The Mann-Whitney U test is a non-parametric alternative that assesses differences between two independent groups. Significance was also determined at the 0.05 alpha level for these tests.

***

Chapter 4: Results

4.1 Stem cell cardiac differentiation under baseline glucose conditions

In this study, pluripotent mESCs were successfully differentiated into three-dimensional, spherical aggregates knowns as embryoid bodies or EBs (**Fig. 3a-c**). The individual cells within the EBs stained positively for the cardiac sarcomeric protein α-actinin 2 (**Fig. 3d**). This successful cardiac differentiation was further confirmed by the onset of spontaneous beating activity within the EBs (see video clip 1, Supplementary Material), a feature unique to cardiac tissue.

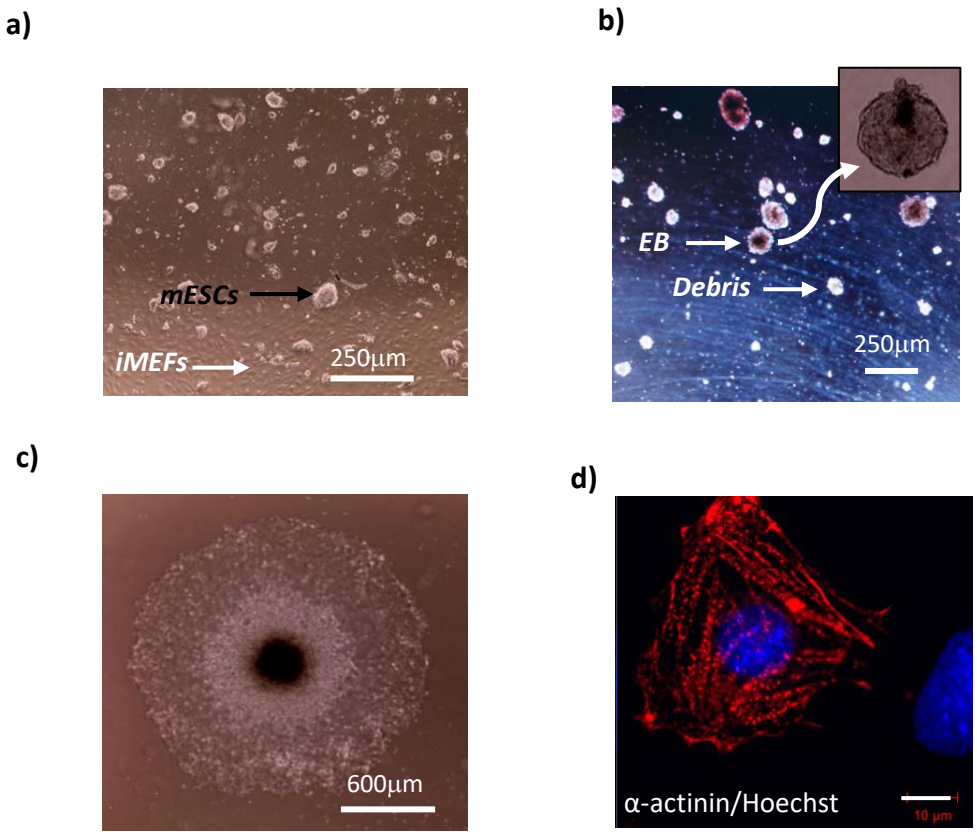

Fig 3. Stem cell cardiac differentiation under baseline glucose conditions. a) Light microscopy image of undifferentiated mouse embryonic stem cells (mESCs) cultured on inactivated mouse embryonic fibroblast (iMEF) feeder layers, viewed under 4X magnification. b) Light microscopy image of a cluster of Day 4-7 embryoids bodies (EBs) as well as some cellular debris in suspension culture. (*Inset*: Zoomed in image of a single EB in suspension culture under 4X magnification) c) Still image of a mature, beating EB under baseline (25 mM) glucose conditions, as seen under light microscopy at 2X magnification. d) Confocal microscopy merged image of a cell dissociated from an EB and stained with α-actinin 2 and Hoechst (40x magnification; scale bar = 10 µm)

4.1 The effect of high glucose on EB beating characteristics

EBs were monitored daily under normal light microscopy for onset of spontaneous beating activity. The cellular contractions within each EB were recorded and converted into a graphical output of amplitude of contraction over time (**Fig. 4b**), using a motion detecting macro on ImageJ, called Myocyter™ (Grune *et al.*, 2019). This study found that the proportion of mature EBs which developed pulsatile activity (relative to the total number of mature EBs within each group) was significantly lower in the high glucose group compared to baseline (**Fig. 4a**, $p<0.05$ versus 25 mM glucose). Moreover, high glucose was found to significantly reduce the EB beating rate (**Fig. 4b-c**, $p<0.01$ versus 25 mM glucose), without significantly altering the standard deviation of the beat-to-beat interval (**Fig. 4d,** $p>0.05$ versus baseline glucose).

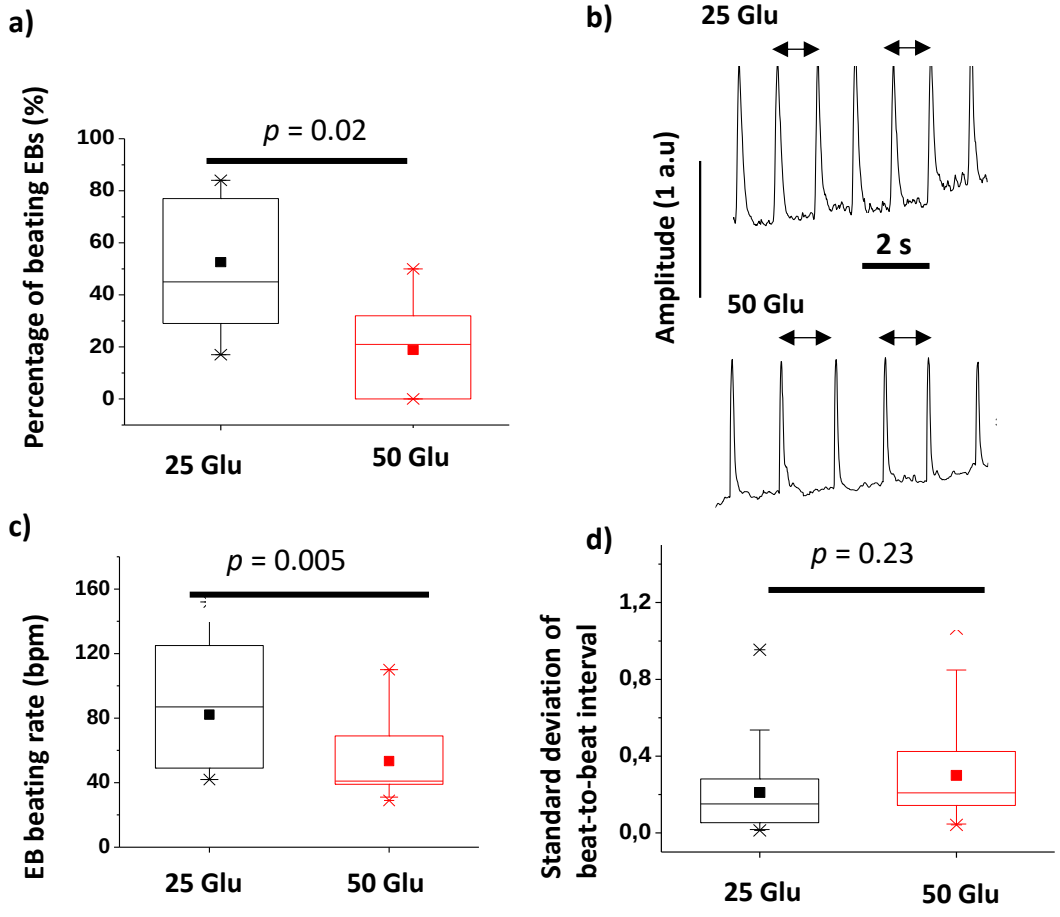

Fig 4. The effect of high glucose on EB beating characteristics. a) Quantitative analysis of the percentage of mature EBs with spontaneous beating activity relative to the total number of EBs within each group ($n\geq$ 14 EBs per group). b) Representative tracings of contractile activity within EBs from each group as detected by Myocyter™. Double arrowheads indicate the duration of a beat-to-beat interval. c-d) Data summaries of EB spontaneous beating rate and standard deviation of the beat-to-beat interval respectively ($n\geq$20 EBs per group, 3 independent cell culture batches). Data are shown as box plot and mean (■). Glu, glucose; a.u., arbitrary unit; bpm, beats per minute

4.2 High glucose and cardiac pacemaker modulation

Given that the spontaneous beating rate of these *in vitro* cardiac cultures is determined by the pacemaker, it can be hypothesized that the reduced beating rate observed under high glucose conditions is due to modulation of the cardiac pacemaker, and the ion channels responsible for generating the cardiac action potential. The funny current (I_f), which is mediated by hyperpolarization-activated cyclic nucleotide-gated (HCN) pacemaker channels, is one of the key contributors to cardiac autorrhythmicity (Choudhury *et al*., 2015). To explore modulation of I_f, EB beating response to ivabradine, a specific HCN channel blocker, was assessed. Application of ivabradine (10 μM) reduced the EB beating rate as expected in cardiac cells, but this ivabradine-induced rate reduction was not found to be significantly different between baseline and high glucose EBs (**Fig.5a-b**, $p>0.05$ versus 25 mM glucose). This finding was further substantiated by Western blot analysis of HCN 4, the main HCN isoform in the mammalian heart, which was not significantly altered by high glucose (**Fig.5c-d**, $p>0.05$ versus 25 mM glucose).

Next, the sensitivity of the pacemaker tissue to β-adrenergic stimulation was tested by applying isoprenaline (12 μM) and recording the EB beating response (**Fig.5d-e**). There was an isoprenaline-induced increase in beating rate under baseline glucose, as expected in cardiac cells, but the change was not significantly attenuated by high glucose ($p>0.05$ versus 25 mM glucose).

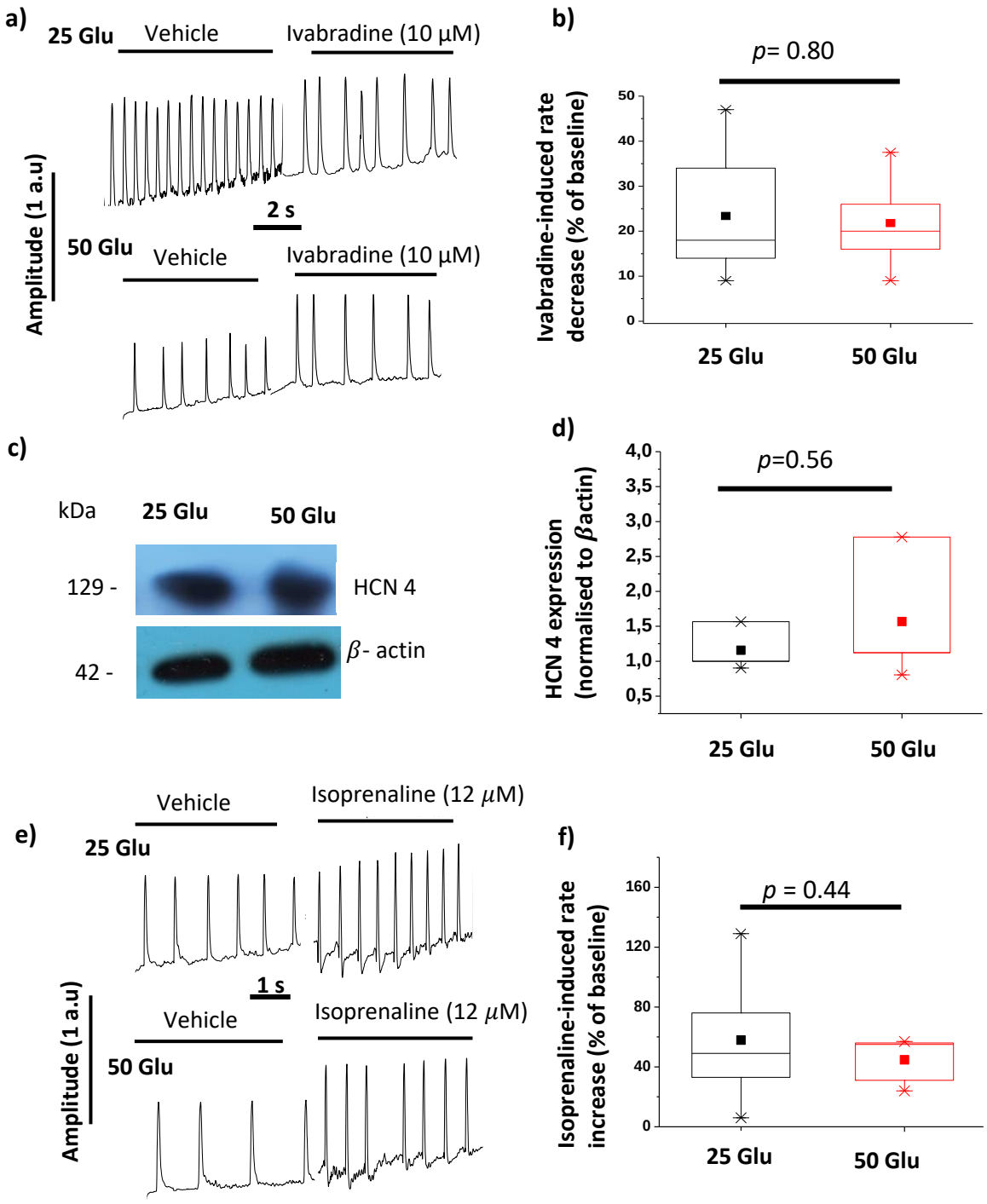

Fig 5. Effect of high glucose on the modulation of pacemaker activity. a) Representative tracings of EB pulsatile activity before and after application of ivabradine (10 μM). b) Summary data of the percentage changes in EB beating rate induced by ivabradine (10 µM; n=8 EBs per group, 2 independent cell culture batches). c) Representative Western blot image of HCN4 and housekeeping protein β-actin. d) Summary data of HCN4 expression normalised to β-actin (n=3 replicates). e) Representative tracings of EB pulsatile activity before and after application of isoprenaline (12 μM). f) Data summary of isoprenaline-induced beating rate increase (12 μM; n≥6 EBs per group, 2 independent cell culture batches). Data are shown as box plot and the mean (■). Glu, glucose.

4.3 The effect of high glucose on propensity to arrhythmogenesis

Arrhythmias are a frequent complication occurring in the diabetic heart, both in the clinical setting and in animal studies. To assess whether EBs grown under high glucose conditions are more prone to rhythm disturbances, the occurrence of ectopic beats was analysed using Myocyter™ tracings derived from time-lapse images of beating EBs. An ectopic beat was identified by its abnormal morphology as seen in **Fig.6a** (black arrowhead). Premature and additional beats, which occurred less frequently, were also counted as ectopic. In this study, there was no significant difference in the occurrence of baseline ectopic beats between the two groups (**Fig. 6b**, p>0.5 versus 25 mM glucose). To further unmask an underlying susceptibility to cardiac arrhythmia, EBs were stimulated with the pro-arrhythmogenic drugs isoprenaline (12 μM) and KCl (12.5 mM), and the occurrence of inducible ectopic beats recorded. The occurrence of KCl and isoprenaline-induced ectopic beats was not significantly different between the two groups (**Fig. 6c-d**, p>0.05 versus 25 mM glucose).

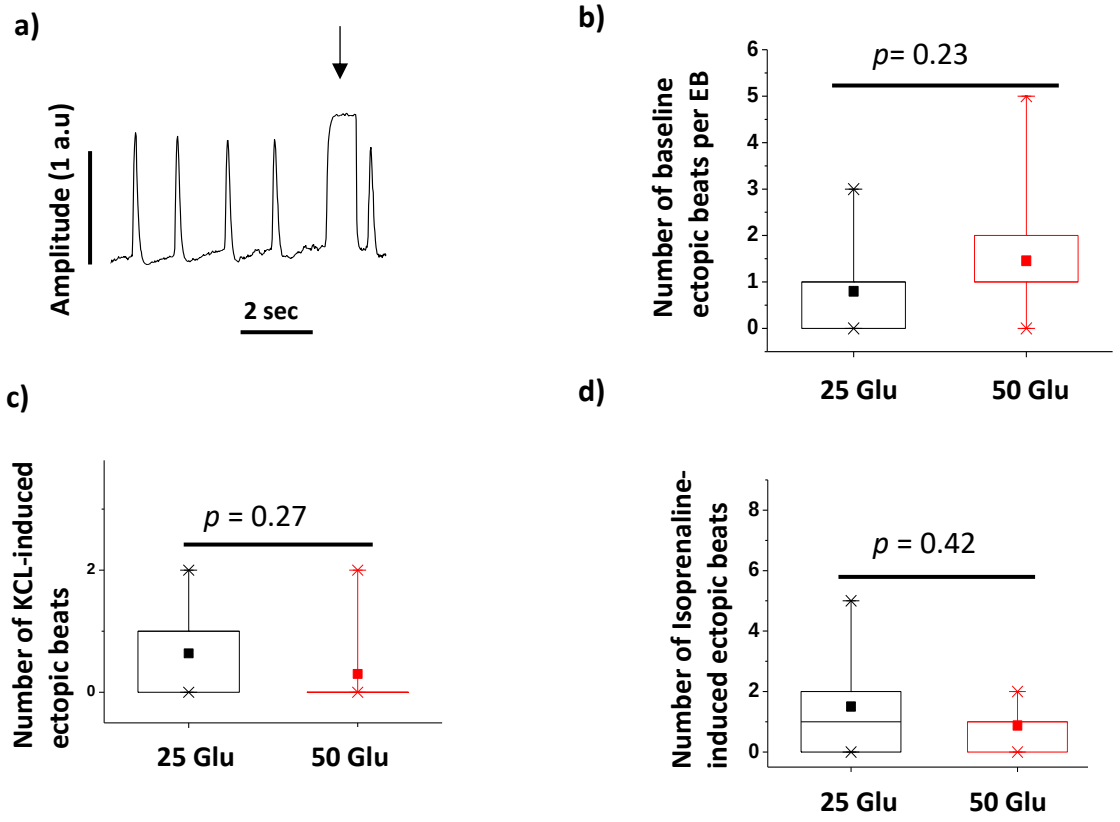

Fig 6. Effect of high glucose on propensity to arrhythmogenesis. a) Representative Myocyter™ tracing showing the typical morphological appearance of an ectopic beat (black arrowhead). b) Quantitative analysis of number of ectopic beats under baseline conditions (n>5 EBs per group). c-d) Summary data of KCl (12.5 mM) and isoprenaline- (12 μM) induced ectopic beats (n>7 EBs per group). Data are shown as box plot and the mean (■). Glu, glucose

4.4 High glucose and sensitivity to quinidine

Uncontrolled hyperglycaemia has been heavily implicated in cardiac electrophysiological remodelling (Grisanti, 2018). To screen for underlying changes in ionic currents other than I_f, EB sensitivity to the multichannel (voltage-gated Na^+ and K^+) blocker quinidine was assessed (**Fig. 7a**). EBs were recorded at 2-minute intervals following application of quinidine (1 μm), and the time to onset of asystole documented. The results indicate an increased sensitivity to quinidine, and a greater propensity towards asystole, the most severe form of cardiac dysrhythmia, under high glucose conditions. This is evidenced by the significantly shorter time period to onset of asystole (**Fig. 7b**, $p<0.05$ versus 25 mM glucose).

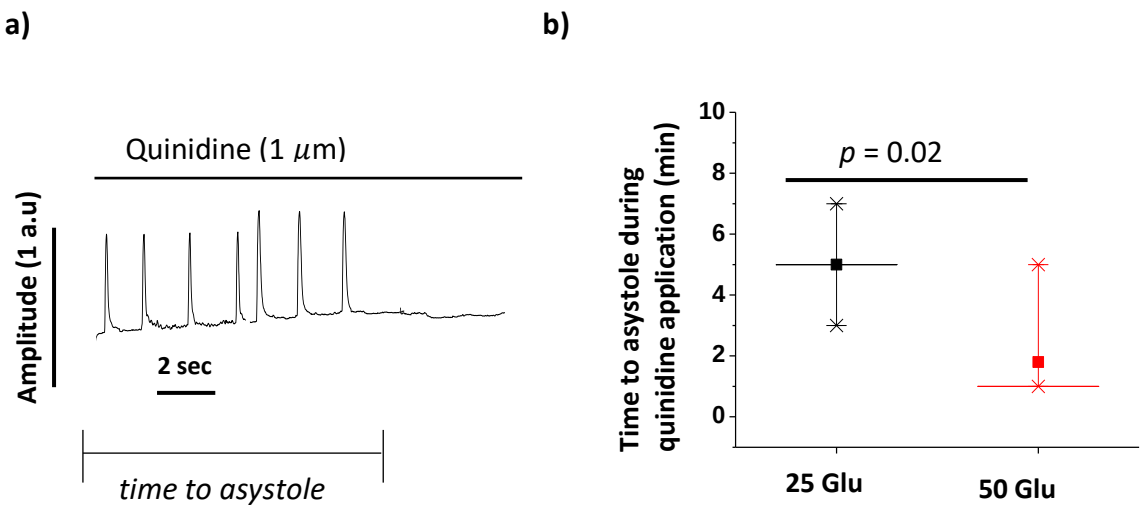

Fig 7. The effect of high glucose on quinidine sensitivity. a) Representative tracing of EB pulsatile activity immediately after application of quinidine (1 μm). b) Data summary of time to onset of asystole following quinidine application (1 μm, n= 6 EBs per group, 2 independent cell culture batches). Data are shown as box plot and the mean (■). Glu, glucose.

4.5 Effect of hyperglycaemia on cardiac intercellular communication

Given that in the clinical setting, diabetes is frequently associated with disturbances of the cardiac conduction system (Wright *et al*., 2012), this study then sought to ascertain whether an impairment in impulse propagation may not better explain the suppressed pulsatile activity observed under high glucose conditions. Although the size of the beating area was not altered by high glucose (**Fig.8a-b**, $p>0.05$ versus 25 mM glucose), there was evidence of impaired gap junction intercellular communication (GJIC), as shown by the significantly reduced lucifer yellow dye transfer distance (**Fig.8c-d**, $p<0.05$ versus 25 mM glucose).

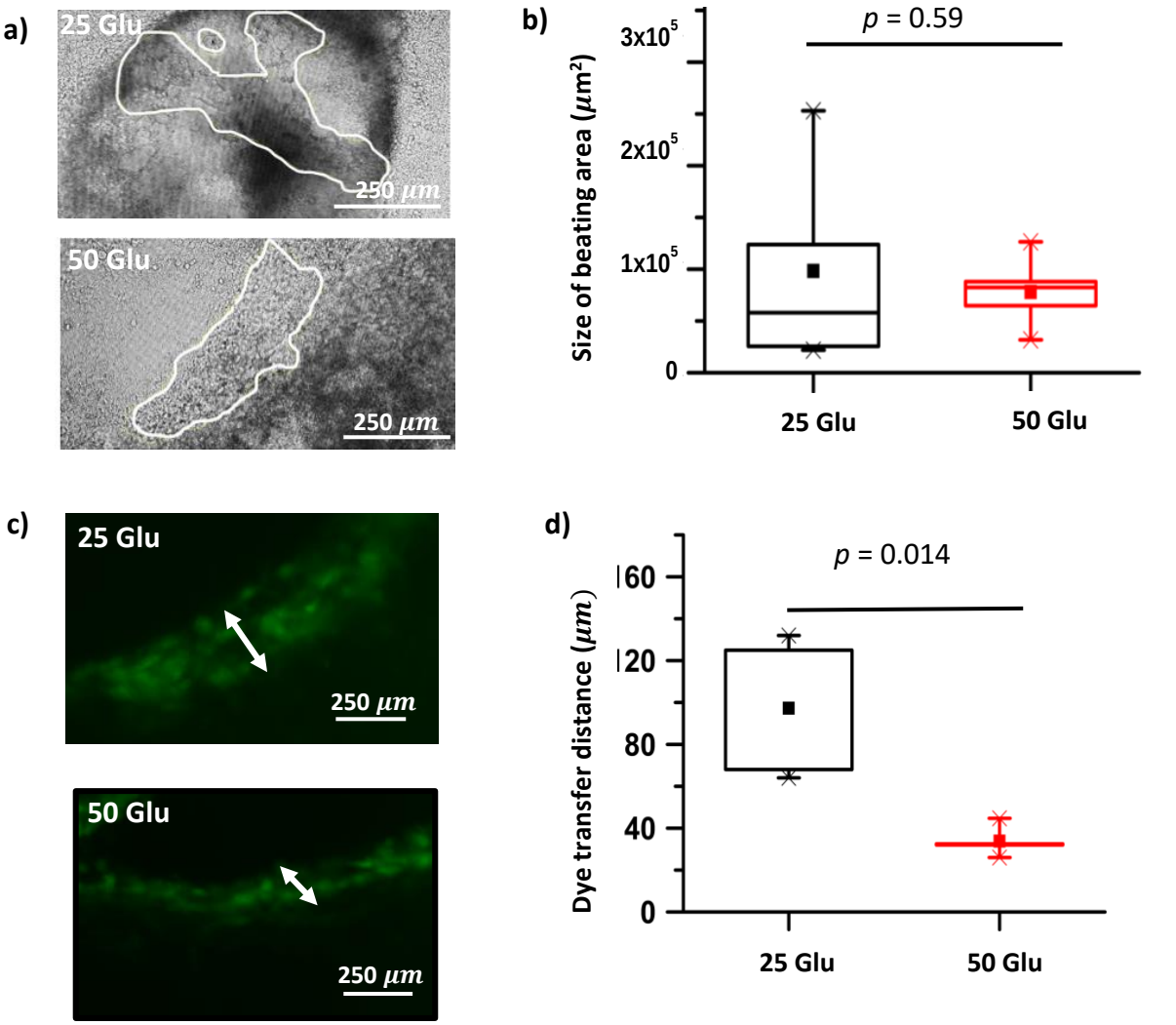

Fig 8. The effect of high glucose on gap junction intercellular communication (GJIC). a) Light microscopy images of beating EBs, with the beating area outlined in white. b) Quantitative analysis of size of EB beating area (n=8 EBs per group). c) Lucifer yellow dye fluorescence signals in individual EBs, post scrape loading of the dye. Double arrowheads indicate distance of dye transfer. d) Quantitative analysis of dye transfer distance (n=5 EBs per group, 3 independent cell culture batches). Data are represented as box plots and mean (■). Glu, glucose.

4.6 High glucose and cardiac connexin-43 expression

To provide a molecular basis for the observed functional impairment in intercellular communication, we then used Western blot analysis and immunocytochemistry (ICC) to analyse the expression and localisation of connexin (Cx)-43, the major cardiac gap junctional protein in the mammalian heart. Interestingly, on Western blot analysis, Cx-43 was detected in all the baseline glucose EBs, whereas it was only detectable in one high glucose EB (**Fig.9a**). Semi-quantitative analysis shows that this protein was significantly reduced by high glucose (**Fig.9b**, $p<0.05$ versus 25 mM glucose). A similar phenomenon was observed on ICC qualitative analysis (**Fig.9c**), where all EBs grown under baseline glucose conditions expressed Cx-43, and less than 50% of the high glucose EBs stained positive for this gap junction protein. In both these instances, the housekeeping proteins, α-actinin and α-tubulin, were stably expressed in all EBs.

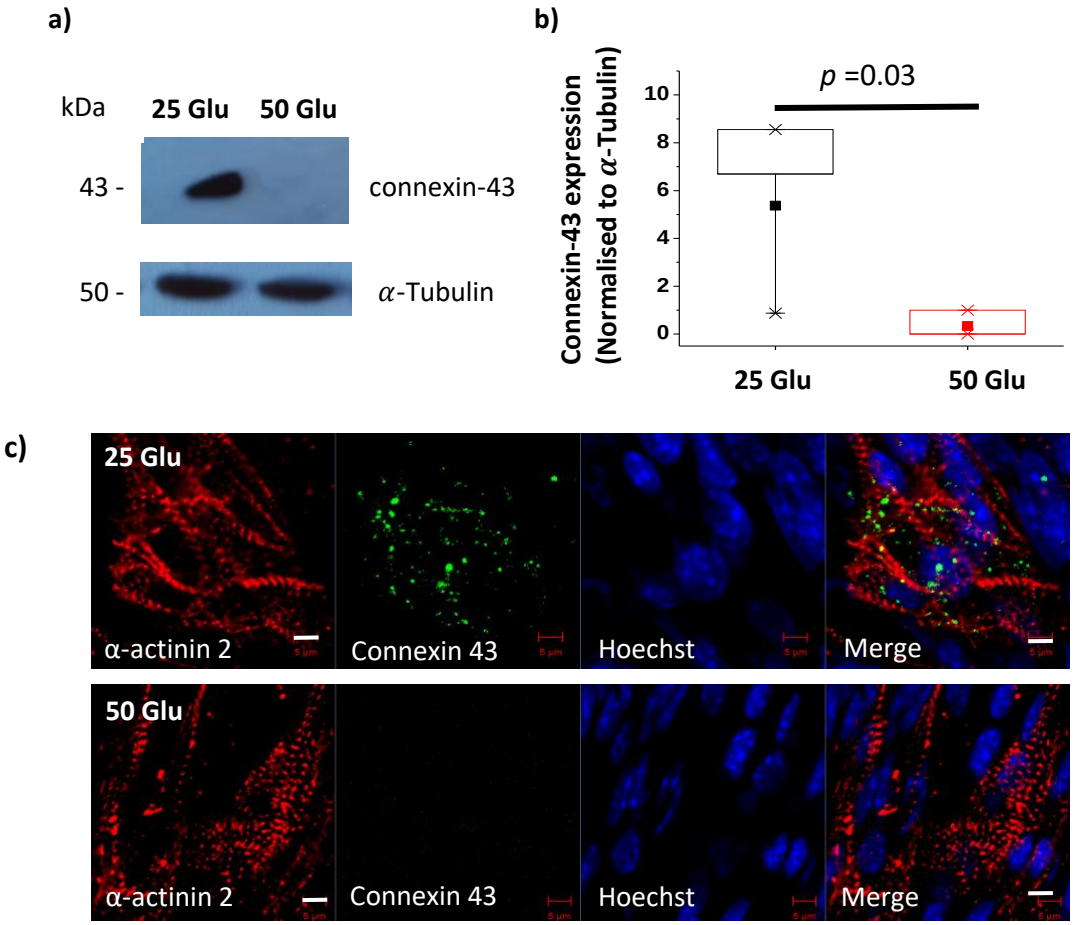

Fig 9. The effect of high glucose on cardiac connexin (Cx)-43 expression. a) Immunoblot image of Cx-43 and housekeeping protein α-Tubulin. Notice the lack of Cx-43 signal in the high glucose group. b) Summary data of Cx-43 expression normalised to α-Tubulin (*n*= 3 replicates). c) Representative confocal microscopy images of α-actinin 2, Cx-43, Hoechst, and merged images. Scale bar = 5 µm. Again, notice the lack of Cx-43 signal in high glucose. Cx-43 was detected in each of the 7 EBs under baseline glucose, but only in 2 out of 5 EBs in high glucose). Data are represented as box plots and mean (■). Glu, glucose.

4.7 Effect of high glucose on transforming growth factor beta 1 (TGF-β1) signalling cascade

To explore whether hyperglycaemia-induced foetal cardiac remodelling involves modulation of the TGF-β signalling pathway, the expression of TGF-β1 and its downstream effector, phosphorylated Smad3 (p-Smad3) were analysed through Western blot. Both TGF-β1 (**Fig. 10a, c**) and p-Smad3 (**Fig. 10b, d**) were significantly upregulated in the high glucose group (p<0.05 versus baseline glucose).

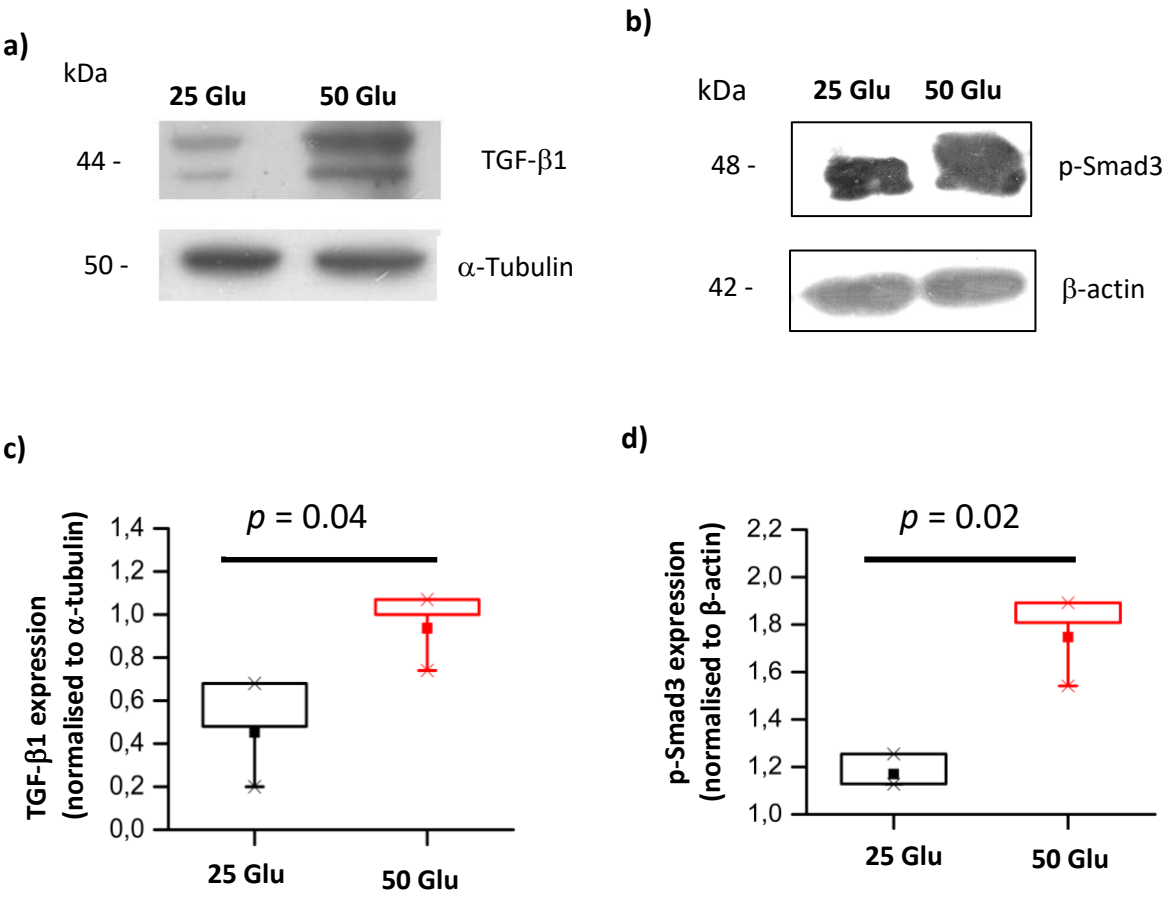

Fig. 10. Effect of high glucose on the transforming growth factor beta 1 (TGF-β1)/Smad3 cascade. a, b) Representative Western blot images of TGF-β1 and phosphorylated Smad3 (p-Smad3) and the housekeeping proteins α-tubulin and β-actin. b, d) Summary data of TGF-β1 expression normalised to α-tubulin (n=3 replicates per group) and of p-Smad3 normalised to β-actin (n=3 replicates per group). Data are shown as box plot and the mean (■). Glu, glucose

Chapter 5: Discussion

The present study demonstrated successful cardiac differentiation of mESCs, as was shown by the onset of spontaneous pulsatile activity within the EBs, and the expression of cardiac-specific markers such as α-actinin 2 and Cx43. The pulsatile areas within the EBs also responded appropriately to cardioactive drugs such as isoprenaline and ivabradine, further supporting the presence of cardiac-like cells. Consistent with previous *in vitro* studies on mESCs (Yang *et al.*, 2016; Aboalgasm *et al.*, 2021), the present study also showed that high glucose has an inhibitory effect on the cardiac differentiation of mESCs as evidenced by the significantly lower proportion of EBs which developed spontaneous pulsatile activity in this group. In other studies, hyperglycaemic conditions during cell culture have been shown to suppress cardiogenesis through downregulation of key developmental genes involved in cardiomyocyte formation, including the major cardiac transcription factor, Kkx2.5 (Han *et al.*, 2015; Yang *et al.*, 2016).

Furthermore, the present study showed that high glucose suppresses the autorrhythmicity of mESC-derived cardiac-like cells, as was demonstrated by the significantly lower spontaneous beating rates. This finding is in keeping with those of numerous animal studies, in which diabetic rats and mice consistently display slower heart rates both *in vivo* and in isolated perfused hearts (Howarth *et al*., 2007; Ferdous *et al*., 2016; Huang *et al*., 2017). In previous animal studies, pacemaker cells isolated from diabetic rat hearts have shown large fluctuations in the beat-to-beat intervals, which clinically manifested as arrhythmias (Albarado-Ibañez *et al.*, 2013; Soltysinska *et al.*, 2014). In the present study, however, high glucose did not significantly alter the beat rate variability, indicating that despite the reduced firing rate, the cardiac pacemaker was still able to rhythmically generate action potentials.

Interestingly, the suppressed autorrhythmicity observed in this study could not be explained by structural or function modulation of the major pacemaker current I_f, given that neither the sensitivity of the pacemaker tissue to HCN channel blocker, ivabradine, nor the protein

expression of the HCN4 channel were significantly altered by high glucose. In previous studies, pacemaker tissue isolated from adult diabetic rats showed a diminished response to ivabradine, an observation which was further supported by the finding of reduced HCN channel expression (Kennedy *et al.*, 1993; Huang *et al.*, 2017; Howarth *et al.*, 2018). Findings from these animal studies have not always been consistent, however, with one study reporting unchanged HCN 4 levels in the diabetic pacemaker (Ferdous *et al.*, 2016), and yet another study reporting an increase in I_f current density (Albarado-Ibañez *et al.*, 2013). Interspecies variation as well as differences in the type of experimental diabetes being induced are likely the cause of this lack of consistency. Importantly, even though there was no demonstrable evidence of I_f modulation under high glucose conditions, this study cannot exclude underlying changes in other cellular pacemaking mechanisms, particularly the Calcium clock.

Hyperglycaemia is a major risk multiplier for cardiac dysrhythmias, both in the adult and developing heart (Arslan *et al.*, 2014; Agarwal and Singh, 2017). In the current study, high glucose was not found to significantly enhance the occurrence of ectopic or abnormal beats. Moreover, in contrast with previous studies which showed a much greater inducibility of arrhythmias under diabetic conditions (Liu *et al.*, 2012; Soltysinska *et al.*, 2014), proarrhythmic stimulation with KCl and isoprenaline was not found to unmask any underlying susceptibility to dysrhythmia. Interestingly, EBs grown in high glucose medium were exquisitely sensitive to the multichannel blocker, quinidine, as shown by the significantly increased tendency to drug-induced asystole. Quinidine works primarily by blocking voltage-gated sodium and potassium channels, resulting in prolongation of the action potential duration as well as reduced automaticity and conduction (Tsai-Turton, 2014). An enhanced sensitivity to this drug could, therefore, reflect underlying electrophysiological changes to these ionic currents. In fact, genes encoding various sodium and potassium channels have previously been shown to be altered in both the adult diabetic heart, and in cultured H9c2 cells exposed to high glucose (Han *et al.*, 2015; Ferdous *et al.*, 2016). Taken together, the slower beating rates and increased quinidine sensitivity demonstrated in this study provide evidence of suppressed autorrhythmicity, and an increased propensity to asystole, the most severe form of dysrhythmia, under high glucose conditions.

Gap junction remodelling is a common feature in many cardiac pathologies (Lin *et al.*, 2006). The present study has provided functional and structural evidence of impaired gap junction communication in embryonic cardiac-like cells exposed to high glucose. This evidence was in the form of a significantly reduced lucifer yellow dye transfer distance, and the downregulation of the major cardiac gap junction protein Cx43. Animal studies have consistently provided evidence of gap junction remodelling in the diabetic heart, with some showing downregulation of all the cardiac connexin isoforms, and others showing structural disruption of gap junction organisation such as lateralisation or internalisation of connexin proteins (Howarth *et al.*, 2007; Nygren *et al.*, 2007; Ferdous *et al.*, 2016). The hyperphosphorylation and enhanced proteolytic degradation of Cx43 have also been implicated in this hyperglycaemia-induced gap junction remodelling (Lin *et al.*, 2006). However, the above-mentioned studies were carried out in the adult diabetic heart, and whether hyperglycaemia has a similar effect on the developing embryonic heart remains largely unknown. In one study, H9c2 rat embryonic cardiomyocytes cultured in high glucose showed reduced Cx43 expression, however because these cells do not display spontaneous pulsatile activity *in vitro*, the functional significance of this connexin remodelling remained unexplored (Han *et al.*, 2015). In the present study, a downregulation of Cx43 resulting in impaired electrical coupling of cardiac cells and slowing of conduction, could, theoretically, explain the slower beating rates observed in high glucose EBs. This study did not assess the effect of hyperglycaemia on the expression of other cardiac connexin isoforms, such as Cx40 and Cx45, which although expressed within the cardiac conduction system, are less abundant compared to Cx43. The downregulation of Cx43 observed in this study could, in theory, be accompanied by a compensatory upregulation of a different connexin isoform with a lower unitary conductance than Cx43, which would result in delayed propagation of the cardiac impulse (Jansen *et al.*, 2010).

The present study has provided some mechanistic insight into the hyperglycaemia-induced pathological remodelling of the electrical conduction system. Cardiac fibrosis is a prominent feature of the diabetic heart, one which has been directly implicated in the pathogenesis of arrhythmias (Wu *et al*., 2018). In this study, consistent with previous animal studies (Liu *et al.*, 2012; Zhang *et al.*, 2019), hyperglycaemia was shown to activate the pro-fibrotic TGF-

$\beta 1$/Smad3 signalling pathway, which could, theoretically, suppress spontaneous beating activity in several ways. Firstly, one of the important cellular effects of TGF-$\beta 1$ is to induce cardiomyocyte hypertrophy, which could contribute to conduction delays through increased cellular axial resistance (Dobaczewski *et al*., 2011). Secondly, TGF-$\beta 1$-mediated fibrosis may physically disrupt electrical coupling between cardiomyocytes, further contributing to impaired signal propagation (Liu *et al.*, 2012). Although TGF-$\beta 1$ and its downstream effector, phosphorylated Smad3, are consistently upregulated in the adult diabetic heart (Jia *et al.*, 2020), findings from experimental models of gestational diabetes have been somewhat contradictory. TGF-$\beta 1$ signalling plays a critical role in cardiac development during the early embryonic period (Zhao, 2010), and maternal hyperglycaemia has been shown to suppress TGF-$\beta 1$/Smad3 and cause cardiac defects in mouse embryos (Wang *et al*., 2015). In another study, however, hyperglycaemia was found to upregulate cardiac TGF-$\beta 1$ expression and cause increased extracellular matrix deposition (Smoak, 2004), a finding which is more in keeping with the pathological remodelling seen in the adult diabetic heart. Given that TGF-β expression patterns change throughout the cardiac developmental process (Zhao, 2010), it is possible that the inhibitory effect of maternal hyperglycaemia on TGF-$\beta 1$ signalling in early embryonic life may later have the opposite effect, though this hypothesis would require further clarification.

Overall, this study has shown, using a cellular developmental model of the heart, that exposure to high glucose suppresses cardiac autorrhythmicity and impairs gap junction-mediated impulse propagation. Moreover, these effects are likely mediated by the profibrotic TGF-$\beta 1$/Smad3 cascade, although this would need to be confirmed through pharmacological inhibition of this signalling pathway. The difficulty in this strategy is that blocking TGF-$\beta 1$ signalling may have adverse, off-target effects, given the crucial role of this multifunctional cytokine in early cardiac development. Even in the process of embryoid body formation, TGF-β is one of the key developmental signalling pathways which are activated by stem cell aggregation (Zeevaert *et al.*, 2020). This limitation may perhaps be overcome through short-term inhibition of the TGF-$\beta 1$/Smad3 cascade in mature EBs, so as to avoid any unwanted adverse effects on cardiac development and maturation.

Limitations of this study

As mentioned in the Methods section, the standard glucose concentration used in mouse embryonic stem cell culture protocols is 25 mM (Wang and Yang, 2008), which is already supraphysiological with regards to normal blood glucose levels. The high glucose concentration of 50 mM which was used in this and in previous *in vitro* studies (Han *et al.*, 2015; Aboalgasm *et al.*, 2021). Nonetheless, the findings of this study need to be interpreted with caution, and validation using an *in vivo* model is necessary.

Another major limitation of this study model is the presence of non-cardiac cell lines with unknown characteristics within each EB. For instance, the contribution of these non-cardiac cells to the overall TGF-$\beta 1$/Smad3 expression levels cannot be excluded. Interestingly, even within the heart itself, cardiomyocytes only account for roughly 30% of the total cell population, with fibroblasts, endothelial cells and pericytes making up the bulk of the cellular landscape (Litviňuková *et al.*, 2020). By minimising EB to EB heterogeneity, this study was able to ensure that the degree of non-cardiac contamination was kept relatively stable and similar across both groups. Hanging drop culture is a validated and reliable method of producing a homogenous and predictable population of EBs (Chen *et al.*, 2011). This is achieved by having a fixed starting number of mESCs seeded into each hanging drop. Furthermore, by ensuring that each well in the culture dishes was occupied by a single EB, this study avoided the unknown effects of EB-to-EB interaction. Nevertheless, some degree of inter-EB variability is unavoidable in this particular study model. Given that these slight differences would be equally distributed across the two experimental groups, this may be considered a form of 'physiological' variation and thus not be expected to affect the overall interpretation of the study's findings.

Lastly, an inherent limitation of all *in vitro* experimentation is that it can never fully capture the complexity of *in vivo* conditions, and so the findings of this study cannot be readily translated into the clinical setting. Unlike traditional monolayer cultures, however, EB spheroids have a complex, three-dimensional (3D) organisation which promotes cell-

extracellular environment interactions, making them somewhat of an intermediate between 2D culture and animal models (Zeevaert *et al.*, 2020). Nonetheless, the findings of this present study would need to be validated using an *in vivo* experimental model.

Future directions

Further electrophysiological characterisation of mESC-derived cardiac cells is required to clarify some of the observations made in the present study. Firstly, the increased quinidine sensitivity of the high glucose EBs, which suggests underlying changes in Na^+ and K^+ voltage-gated currents. Secondly, the lack of I_f modulation despite evidence of suppressed autorrhythmicity, which may be pointing towards impaired intracellular Ca^{2+} cycling instead. Finally, future studies will need to confirm that the TGF-$\beta 1$ cascade is indeed a key driver of pathological cardiac remodelling in the developing heart exposed to hyperglycaemia, and thus a potential therapeutic target.

Conclusion

In this study, hyperglycaemia suppressed the autorrhythmicity and impulse propagation of mESC-derived cardiac-like cells. These cardiotoxic effects were mediated, in part, by activation of canonical TGF-$\beta 1$/Smad3 pathways. With the rising prevalence of pregnancies complicated by maternal diabetes, the findings of this study may have significant clinical implications in foetal diabetic cardiac disease, particularly as it pertains to heart rhythm disturbances. Furthermore, these findings may also provide useful mechanistic insights into the adult diabetic heart and its vulnerability to dysrhythmia, given that foetal cardiac gene reactivation is a key feature of this pathological state.

***

References

Aboalgasm, H. *et al.* (2021) 'Hyperglycaemia-Induced Contractile Dysfunction and Apoptosis in Cardiomyocyte-Like Pulsatile Cells Derived from Mouse Embryonic Stem Cells', *Cardiovascular Toxicology*, 21(9), pp. 695–709. Available at: https://doi.org/10.1007/s12012-021-09660-3.

Aganović, I. and Dušek, T. (2007) 'Pathophysiology of Metabolic Syndrome.', *EJIFCC*, 18(1), pp. 3–6.

Agarwal, G. and Singh, S. (2017) 'Arrhythmias in type 2 diabetes mellitus', *Indian Journal of Endocrinology and Metabolism*. Available at: https://doi.org/10.4103/ijem.IJEM_448_16.

Albarado-Ibañez, A. *et al.* (2013) 'Metabolic Syndrome Remodels Electrical Activity of the Sinoatrial Node and Produces Arrhythmias in Rats', *PLoS ONE*, 8(11), p. e76534. Available at: https://doi.org/10.1371/journal.pone.0076534.

Al-Biltagi, M., el razaky, O. and el Amrousy, D. (2021) 'Cardiac changes in infants of diabetic mothers', *World Journal of Diabetes*, 12(8), pp. 1233–1247. Available at: https://doi.org/10.4239/wjd.v12.i8.1233.

Ali, N.N. *et al.* (2004) 'Beta-adrenoceptor subtype dependence of chronotropy in mouse embryonic stem cell-derived cardiomyocytes', *Basic Research in Cardiology*, 99(6), pp. 382–391. Available at: https://doi.org/10.1007/s00395-004-0484-5.

Antzelevitch, C. and Burashnikov, A. (2011) 'Overview of Basic Mechanisms of Cardiac Arrhythmia', *Cardiac Electrophysiology Clinics*, 3(1), pp. 23–45. Available at: https://doi.org/10.1016/j.ccep.2010.10.012.

Arslan, D. *et al.* (2014) 'Prolonged QT dispersion in the infants of diabetic mothers', *Pediatric Cardiology*, 35(6), pp. 1052–1056. Available at: https://doi.org/10.1007/s00246-014-0897-3.

Aune, D. *et al.* (2018) 'Diabetes mellitus, blood glucose and the risk of atrial fibrillation: A systematic review and meta-analysis of cohort studies', *Journal of Diabetes and its Complications*, 32(5), pp. 501–511. Available at: https://doi.org/10.1016/j.jdiacomp.2018.02.004.

Babica, P., Sovadinová, I. and Upham, B.L. (2016) 'Scrape loading/dye transfer assay', in *Methods in Molecular Biology*. Humana Press Inc., pp. 133–144. Available at: https://doi.org/10.1007/978-1-4939-3664-9_9.

Bucchi, A. *et al.* (2003) 'If-dependent modulation of pacemaker rate mediated by cAMP in the presence of ryanodine in rabbit sino-atrial node cells', *Journal of Molecular and Cellular Cardiology*, 35(8), pp. 905–913. Available at: https://doi.org/10.1016/S0022-2828(03)00150-0.

Chen, M. *et al.* (2011) 'Enrichment of cardiac differentiation of mouse embryonic stem cells by optimizing the hanging drop method', *Biotechnology Letters*, 33(4), pp. 853–858. Available at: https://doi.org/10.1007/s10529-010-0494-3.

Choudhury, M., Boyett, M.R. and Morris, G.M. (2015) 'Biology of the sinus node and its disease', *Arrhythmia and Electrophysiology Review*. Available at: https://doi.org/10.15420/aer.2015.4.1.28.

Coppen, S.R. *et al.* (2003) 'Comparison of connexin expression patterns in the developing mouse heart and human foetal heart.', *Molecular and cellular biochemistry*, 242(1–2), pp. 121–7.

Crispi, F. *et al.* (2020) 'Main Patterns of Fetal Cardiac Remodeling', *Fetal Diagnosis and Therapy*, 47(5), pp. 337–344. Available at: https://doi.org/10.1159/000506047.

Csepe, T.A. *et al.* (2015) 'Fibrosis: A structural modulator of sinoatrial node physiology and dysfunction', *Frontiers in Physiology*, 6(FEB). Available at: https://doi.org/10.3389/fphys.2015.00037.

DiFrancesco, D. (1985) 'The cardiac hyperpolarizing-activated current, if. origins and developments', *Progress in Biophysics and Molecular Biology*, 46(3), pp. 163–183. Available at: https://doi.org/10.1016/0079-6107(85)90008-2.

DiFrancesco, D. (1991) 'The contribution of the "pacemaker" current (if) to generation of spontaneous activity in rabbit sino-atrial node myocytes.', *The Journal of Physiology*, 434(1), pp. 23–40. Available at: https://doi.org/10.1113/jphysiol.1991.sp018457.

Dobaczewski, M., Chen, W. and Frangogiannis, N.G. (2011) 'Transforming growth factor (TGF)-β signaling in cardiac remodeling', *Journal of Molecular and Cellular Cardiology*, 51(4), pp. 600–606. Available at: https://doi.org/10.1016/j.yjmcc.2010.10.033.

D'Souza, A. *et al.* (2017) 'Targeting miR-423-5p Reverses Exercise Training-Induced HCN4 Channel Remodeling and Sinus Bradycardia', *Circulation Research*. Available at: https://doi.org/10.1161/CIRCRESAHA.117.311607.

Dunachie, S. and Chamnan, P. (2019) 'The double burden of diabetes and global infection in low and middle-income countries', *Transactions of the Royal Society of Tropical Medicine and Hygiene*. Available at: https://doi.org/10.1093/trstmh/try124.

Einarson, T.R. *et al.* (2018) 'Prevalence of cardiovascular disease in type 2 diabetes: A systematic literature review of scientific evidence from across the world in 2007-2017', *Cardiovascular Diabetology*. Available at: https://doi.org/10.1186/s12933-018-0728-6.

Fahrenbach, J.P., Mejia-Alvarez, R. and Banach, K. (2007) 'The relevance of non-excitable cells for cardiac pacemaker function', *Journal of Physiology*, 585(2), pp. 565–578. Available at: https://doi.org/10.1113/jphysiol.2007.144121.

Ferdous, Z. *et al.* (2016) 'Different Profile of mRNA Expression in Sinoatrial Node from Streptozotocin-Induced Diabetic Rat', *PLOS ONE*, 11(4), p. e0153934. Available at: https://doi.org/10.1371/journal.pone.0153934.

Gaztañaga, L., Marchlinski, F.E. and Betensky, B.P. (2012) 'Mecanismos de las arritmias cardiacas', *Revista Espanola de Cardiologia*. Available at: https://doi.org/10.1016/j.recesp.2011.09.018.

Grisanti, L.A. (2018) 'Diabetes and Arrhythmias: Pathophysiology, Mechanisms and Therapeutic Outcomes', *Frontiers in Physiology*. Available at: https://doi.org/10.3389/fphys.2018.01669.

Grune, T. *et al.* (2019) 'The "MYOCYTER" – Convert cellular and cardiac contractions into numbers with ImageJ', *Scientific Reports*, 9(1), p. 15112. Available at: https://doi.org/10.1038/s41598-019-51676-x.

Guthrie, R.A. and Guthrie, D.W. (2004) *Pathophysiology of Diabetes Mellitus*, *Crit Care Nurs Q*, 27(2): p.113-125. Available at: https//doi.org/10.1097/00002727-200404000-00003

Han, S. *et al.* (2015) 'Investigating the Mechanism of Hyperglycemia-Induced Fetal Cardiac Hypertrophy', *PLOS ONE*, 10(9), p. e0139141. Available at: https://doi.org/10.1371/journal.pone.0139141.

Han, S.S. *et al.* (2015) 'Investigating the mechanism of hyperglycemia-induced fetal cardiac hypertrophy', *PLoS ONE*, 10(9). Available at: https://doi.org/10.1371/journal.pone.0139141.

Hoodbhoy, Z. *et al.* (2019) 'Is the child at risk? Cardiovascular remodelling in children born to diabetic mothers', *Cardiology in the Young*, 29(4), pp. 467–474. Available at: https://doi.org/10.1017/S1047951119000040.

Howarth, F. Chris *et al.* (2007) 'Altered expression of gap junction connexin proteins may partly underlie heart rhythm disturbances in the streptozotocin-induced diabetic rat heart',

Molecular and Cellular Biochemistry, 305(1–2), pp. 145–151. Available at: https://doi.org/10.1007/s11010-007-9537-z.

Howarth, F. C. *et al.* (2007) 'Effects of streptozotocin-induced diabetes on action potentials in the sinoatrial node compared with other regions of the rat heart', *Molecular and Cellular Biochemistry*, 300(1–2), pp. 39–46. Available at: https://doi.org/10.1007/s11010-006-9366-5.

Howarth, F.C. *et al.* (2018) 'The Pattern of mRNA Expression Is Changed in Sinoatrial Node from Goto-Kakizaki Type 2 Diabetic Rat Heart', *Journal of Diabetes Research*. Available at: https://doi.org/10.1155/2018/8454078.

Huang, X. *et al.* (2017) 'Reduced expression of HCN channels in the sinoatrial node of streptozotocin-induced diabetic rats', *Canadian Journal of Physiology and Pharmacology*, 95(5), pp. 586–594. Available at: https://doi.org/10.1139/cjpp-2016-0418.

Humphrey, R.K. (2004) 'Maintenance of Pluripotency in Human Embryonic Stem Cells Is STAT3 Independent', *Stem Cells*. Available at: https://doi.org/10.1634/stemcells.22-4-522.

Janse, M. (2004) 'Electrophysiological changes in heart failure and their relationship to arrhythmogenesis', *Cardiovascular Research*, 61(2), pp. 208–217. Available at: https://doi.org/10.1016/j.cardiores.2003.11.018.

Jansen, J.A. *et al.* (2010) 'Cardiac connexins and impulse propagation', *Journal of Molecular and Cellular Cardiology*, 48(1), pp. 76–82. Available at: https://doi.org/10.1016/j.yjmcc.2009.08.018.

Jia, X. *et al.* (2020) 'TRPV4 Mediates Cardiac Fibrosis via the TGF-β1/Smad3 Signaling Pathway in Diabetic Rats', *Cardiovascular Toxicology*, 20(5), pp. 492–499. Available at: https://doi.org/10.1007/s12012-020-09572-8.

Jongbloed, M.R.M. *et al.* (2004) 'Embryonic Conduction Tissue':, *Journal of Cardiovascular Electrophysiology*, 15(3), pp. 349–355. Available at: https://doi.org/10.1046/j.1540-8167.2004.03487.x.

Joung, B. *et al.* (2009) 'The Calcium and Voltage Clocks in Sinoatrial Node Automaticity', *Korean Circulation Journal*, 39(6), p. 217. Available at: https://doi.org/10.4070/kcj.2009.39.6.217.

Kennedy, R.H. *et al.* (1993) 'Effects of cesium on spontaneous rate in right atria isolated from diabetic rats', *Canadian Journal of Physiology and Pharmacology*, 71(9), pp. 675–678. Available at: https://doi.org/10.1139/y93-099.

Kornblum, A. *et al.* (2013) 'A New Model to Perform Electrophysiological Studies in the Early Embryonic Mouse Heart', *Cellular Physiology and Biochemistry*, 32(1), pp. 1–10. Available at: https://doi.org/10.1159/000350118.

Kuwabara, Y. *et al.* (2013) 'Increased Expression of HCN Channels in the Ventricular Myocardium Contributes to Enhanced Arrhythmicity in Mouse Failing Hearts', *Journal of the American Heart Association*, 2(3). Available at: https://doi.org/10.1161/JAHA.113.000150.

Lázár, E., Sadek, H.A. and Bergmann, O. (2017) 'Cardiomyocyte renewal in the human heart: insights from the fall-out', *European Heart Journal*, 38(30), pp. 2333–2342. Available at: https://doi.org/10.1093/eurheartj/ehx343.

Lear, J.T., Lawrence, I.G. and Burden, A.C. (1996) 'Prevalance of diabetes in elderly patients requiring permanent cardiac pacemaker insertion', *Acta Diabetologica*. Available at: https://doi.org/10.1007/BF00569430.

Lee, Y.-N. and Huda, M.S. (2021) 'Uncommon forms of diabetes', *Clinical Medicine*, 21(4), pp. e337–e341. Available at: https://doi.org/10.7861/clinmed.2021-0369.

Liang, X., Evans, S.M. and Sun, Y. (2015) 'Insights into cardiac conduction system formation provided by HCN4 expression', *Trends in Cardiovascular Medicine*, 25(1), pp. 1–9. Available at: https://doi.org/10.1016/j.tcm.2014.08.009.

Lin, H. *et al.* (2006) 'Remodeling of connexin 43 in the diabetic rat heart', *Molecular and Cellular Biochemistry*, 290(1–2), pp. 69–78. Available at: https://doi.org/10.1007/s11010-006-9166-y.

Lipsett, D.B. *et al.* (2019) 'Cardiomyocyte substructure reverts to an immature phenotype during heart failure', *The Journal of Physiology*, 597(7), pp. 1833–1853. Available at: https://doi.org/10.1113/JP277273.

Litviňuková, M. *et al.* (2020) 'Cells of the adult human heart', *Nature*, 588(7838), pp. 466–472. Available at: https://doi.org/10.1038/s41586-020-2797-4.

Liu, C. *et al.* (2012) 'Hyperglycemia aggravates atrial interstitial fibrosis, ionic remodeling and vulnerability to atrial fibrillation in diabetic rabbits', *Anadolu Kardiyoloji Dergisi/The Anatolian Journal of Cardiology*. Available at: https://doi.org/10.5152/akd.2012.188.

Mangoni, M.E. and Nargeot, J. (2008) 'Genesis and Regulation of the Heart Automaticity', *Physiological Reviews*, 88(3), pp. 919–982. Available at: https://doi.org/10.1152/physrev.00018.2007.

Mapanga, R.F. and Essop, M.F. (2016) 'Damaging effects of hyperglycemia on cardiovascular function: Spotlight on glucose metabolic pathways', *American Journal of Physiology - Heart and Circulatory Physiology*. Available at: https://doi.org/10.1152/ajpheart.00206.2015.

Mapa-Tassou, C. *et al.* (2019) 'Economic Impact of Diabetes in Africa', *Current Diabetes Reports*, 19(2), p. 5. Available at: https://doi.org/10.1007/s11892-019-1124-7.

Moorman, A.F.M. *et al.* (1998) 'Development of the Cardiac Conduction System', *Circulation Research*, 82(6), pp. 629–644. Available at: https://doi.org/10.1161/01.RES.82.6.629.

Morgan, S.C. *et al.* (2008) 'Oxidative stress during diabetic pregnancy disrupts cardiac neural crest migration and causes outflow tract defects', *Birth Defects Research Part A: Clinical and Molecular Teratology*, 82(6), pp. 453–463. Available at: https://doi.org/10.1002/bdra.20457.

Nakamura, T., Colbert, M.C. and Robbins, J. (2006) 'Neural crest cells retain multipotential characteristics in the developing valves and label the cardiac conduction system.', *Circulation research*, 98(12), pp. 1547–54. Available at: https://doi.org/10.1161/01.RES.0000227505.19472.69.

Nakano, H. *et al.* (2017) 'Glucose inhibits cardiac muscle maturation through nucleotide biosynthesis', *eLife*, 6. Available at: https://doi.org/10.7554/eLife.29330.

Nakano, H., Fajardo, V.M. and Nakano, A. (2021) 'The role of glucose in physiological and pathological heart formation', *Developmental Biology*, 475, pp. 222–233. Available at: https://doi.org/10.1016/j.ydbio.2021.01.020.

Nygren, A. *et al.* (2007) 'Propagation of the cardiac impulse in the diabetic rat heart: reduced conduction reserve', *The Journal of Physiology*, 580(2), pp. 543–560. Available at: https://doi.org/10.1113/jphysiol.2006.123729.

Ogedengbe, S.O. and Ezeani, I.U. (2014) 'Profile of metabolic abnormalities seen in patients with type 2 diabetes mellitus and their first degree relatives with metabolic syndrome seen in Benin City, Edo state Nigeria', *Journal of Diabetes & Metabolic Disorders*, 13(1), p. 61. Available at: https://doi.org/10.1186/2251-6581-13-61.

Ogurtsova, K. *et al.* (2022) 'IDF diabetes Atlas: Global estimates of undiagnosed diabetes in adults for 2021', *Diabetes Research and Clinical Practice*, 183, p. 109118. Available at: https://doi.org/10.1016/j.diabres.2021.109118.

Paff, G.H., Boucek, R.J. and Harrell, T.C. (1968) 'Observations on the development of the electrocardiogram', *The Anatomical Record*, 160(3), pp. 575–581. Available at: https://doi.org/10.1002/ar.1091600306.

Park, D.S. and Fishman, G.I. (2011) 'The Cardiac Conduction System', *Circulation*, 123(8), pp. 904–915. Available at: https://doi.org/10.1161/CIRCULATIONAHA.110.942284.

Pheiffer, C. *et al.* (2018) 'The prevalence of type 2 diabetes in South Africa: A systematic review protocol', *BMJ Open*. Available at: https://doi.org/10.1136/bmjopen-2017-021029.

Pike, J.I. *et al.* (2013) 'Fetal and neonatal atrial arrhythmias: an association with maternal diabetes and neonatal macrosomia', *Prenatal Diagnosis*, 33(12), pp. 1152–1157. Available at: https://doi.org/10.1002/pd.4210.

Plows, J. *et al.* (2018) 'The Pathophysiology of Gestational Diabetes Mellitus', *International Journal of Molecular Sciences*, 19(11), p. 3342. Available at: https://doi.org/10.3390/ijms19113342.

Podlaha, R. and Falk, A. (1992) 'The prevalence of diabetes mellitus and other risk factors of atherosclerosis in bradycardia requiring pacemaker treatment', in *Hormone and Metabolic Research, Supplement*.

Porrello, E.R. *et al.* (2011) 'Transient Regenerative Potential of the Neonatal Mouse Heart', *Science*, 331(6020), pp. 1078–1080. Available at: https://doi.org/10.1126/science.1200708.

Rajabi, M. *et al.* (2007) 'Return to the fetal gene program protects the stressed heart: a strong hypothesis', *Heart Failure Reviews*, 12(3–4), pp. 331–343. Available at: https://doi.org/10.1007/s10741-007-9034-1.

Rubenstein, D.S. and Lipsius, S.L. (1989) 'Mechanisms of automaticity in subsidiary pacemakers from cat right atrium.', *Circulation Research*, 64(4), pp. 648–657. Available at: https://doi.org/10.1161/01.RES.64.4.648.

Sartiani, L. *et al.* (2017) 'The hyperpolarization-activated cyclic nucleotide-gated channels: From biophysics to pharmacology of a unique family of ion channels', *Pharmacological Reviews*. Available at: https://doi.org/10.1124/pr.117.014035.

Senges, Jochen *et al.* (1980) '*Altered Cardiac Automaticity and Conduction in Experimental Diabetes Mellitus'*, *Journal of Molecular and Cellular Cardiology*, 12(12), p. 1341-1351. Available at: https://doi:10.1016/0022-2828(80)90120-0

Shankar, P. *et al.* (2019) 'Cardiovascular malformations in infants of diabetic mothers: a retrospective study', *International Journal of Contemporary Pediatrics*, 6(5), p. 1998. Available at: https://doi.org/10.18203/2349-3291.ijcp20193712.

Singh, B.S., Westfall, T.C. and Devaskar, S.U. (1997) 'Maternal Diabetes-Induced Hyperglycemia and Acute Intracerebral Hyperinsulinism Suppress Fetal Brain Neuropeptide Y Concentrations [1]', *Endocrinology*, 138(3), pp. 963–969. Available at: https://doi.org/10.1210/endo.138.3.5001.

Singh, V.P. *et al.* (2008) 'Intracellular angiotensin II production in diabetic rats is correlated with cardiomyocyte apoptosis, oxidative stress, and cardiac fibrosis', *Diabetes*, 57(12), pp. 3297–3306. Available at: https://doi.org/10.2337/db08-0805.

Skyler, J.S. (2004) 'Diabetes Mellitus: Pathogenesis and Treatment Strategies', *Journal of Medicinal Chemistry*, 47(17), pp. 4113–4117. Available at: https://doi.org/10.1021/jm0306273.

Smoak, I.W. (2004) 'Hyperglycemia-induced TGF? and fibronectin expression in embryonic mouse heart', *Developmental Dynamics*, 231(1), pp. 179–189. Available at: https://doi.org/10.1002/dvdy.20123.

Soltysinska, E. *et al.* (2014) 'Sinoatrial node dysfunction induces cardiac arrhythmias in diabetic mice', *Cardiovascular Diabetology*, 13(1), p. 122. Available at: https://doi.org/10.1186/s12933-014-0122-y.

Stoner, G.D. (2017) 'Hyperosmolar Hyperglycemic State.', *American family physician*, 96(11), pp. 729–736.

Tsai-Turton, M. (2014) 'Quinidine', in *Encyclopedia of Toxicology: Third Edition*. Elsevier, pp. 16–18. Available at: https://doi.org/10.1016/B978-0-12-386454-3.00055-5.

Tse, G. *et al.* (2016) 'Molecular and Electrophysiological Mechanisms Underlying Cardiac Arrhythmogenesis in Diabetes Mellitus', *Journal of Diabetes Research*. Available at: https://doi.org/10.1155/2016/2848759.

Van Veen, T.A.B., Van Rijen, H.V.M. and Opthof, T. (2001) 'Cardiac gap junction channels: Modulation of expression and channel properties', *Cardiovascular Research*. Available at: https://doi.org/10.1016/S0008-6363(01)00324-8.

Vinogradova, T.M., Bogdanov, K.Yu. and Lakatta, E.G. (2002) 'β-Adrenergic Stimulation Modulates Ryanodine Receptor Ca $^{2+}$ Release During Diastolic Depolarization to Accelerate Pacemaker Activity in Rabbit Sinoatrial Nodal Cells', *Circulation Research*, 90(1), pp. 73–79. Available at: https://doi.org/10.1161/hh0102.102271.

Wang, F., Reece, E.A. and Yang, P. (2015) 'Oxidative stress is responsible for maternal diabetes-impaired transforming growth factor beta signaling in the developing mouse heart', *American Journal of Obstetrics and Gynecology*, 212(5), pp. 650.e1-650.e11. Available at: https://doi.org/10.1016/j.ajog.2015.01.014.

Wang, X. and Yang, P. (2008) 'In vitro differentiation of mouse embryonic stem (mES) cells using the hanging drop method', *Journal of Visualized Experiments*, (17). Available at: https://doi.org/10.3791/825.

Watanabe, M. *et al.* (2016) 'Probing the Electrophysiology of the Developing Heart', *Journal of Cardiovascular Development and Disease*, 3(1), p. 10. Available at: https://doi.org/10.3390/jcdd3010010.

Wright, J.A., Richards, T. and Becker, D.L. (2012) 'Connexins and Diabetes', *Cardiology Research and Practice*, 2012, pp. 1–8. Available at: https://doi.org/10.1155/2012/496904.

Wu, J., Jackson-Weaver, O. and Xu, J. (2018) 'The TGFβ superfamily in cardiac dysfunction', *Acta Biochimica et Biophysica Sinica*, 50(4), pp. 323–335. Available at: https://doi.org/10.1093/abbs/gmy007.

Yang, B. *et al.* (2020) 'Mitochondrial thioredoxin-2 maintains HCN4 expression and prevents oxidative stress-mediated sick sinus syndrome', *Journal of Molecular and Cellular Cardiology*. Available at: https://doi.org/10.1016/j.yjmcc.2019.10.009.

Yang, P.-C. and Mahmood, T. (2012) 'Western blot: Technique, theory, and trouble shooting', *North American Journal of Medical Sciences*, 4(9), p. 429. Available at: https://doi.org/10.4103/1947-2714.100998.

Yang, Penghua *et al.* (2016) 'High glucose suppresses embryonic stem cell differentiation into cardiomyocytes', *Stem Cell Research & Therapy*, 7(1), p. 187. Available at: https://doi.org/10.1186/s13287-016-0446-5.

Yli, B.M. *et al.* (2008) 'Intrapartum fetal ECG and diabetes', *Journal of Maternal-Fetal and Neonatal Medicine*, 21(4), pp. 231–238. Available at: https://doi.org/10.1080/14767050801924431.

Zeevaert, K. *et al.* (2020) 'Cell Mechanics in Embryoid Bodies', *Cells*, 9(10), p. 2270. Available at: https://doi.org/10.3390/cells9102270.

Zhang, Y. *et al.* (2019) 'Electrical Conduction System Remodeling in Streptozotocin-Induced Diabetes Mellitus Rat Heart', *Frontiers in Physiology*. Available at: https://doi.org/10.3389/fphys.2019.00826.

Zhao, Z. (2010) 'Cardiac malformations and alteration of TGFβ signaling system in diabetic embryopathy', *Birth Defects Research Part B: Developmental and Reproductive Toxicology*, p. n/a-n/a. Available at: https://doi.org/10.1002/bdrb.20225.

Ziad, I. and Miller, J. (2019) 'Electrophysiological Mechanisms of Cardiac Arrhythmias', in *Clinical Arrhythmology and Electrophysiology*. 3rd edn. Philadelphia: Elsevier, pp. 51–80.

Appendix

Section A: Stem cell culture and proliferation

Mycoplasma testing protocol

1)

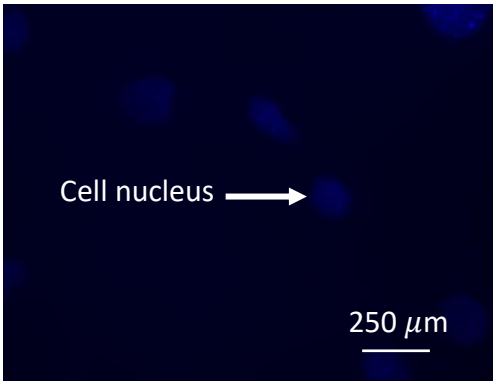

Fig A1. Image of a negative Mycoplasma staining result. mESCs were stained with the Hoechst nuclear dye and visualised under fluorescent microscopy (EVOS™ M5000). As seen in the image above, the large bright blue fluorescence indicates uptake of the Hoechst dye by the cell nucleus (i.e., mESCs). In a contaminated cell culture, Mycoplasma would be detected as small, pinpoint or dot-like areas of blue fluorescence surrounding the nuclei. This would be indicative of a positive Mycoplasma test.

2)

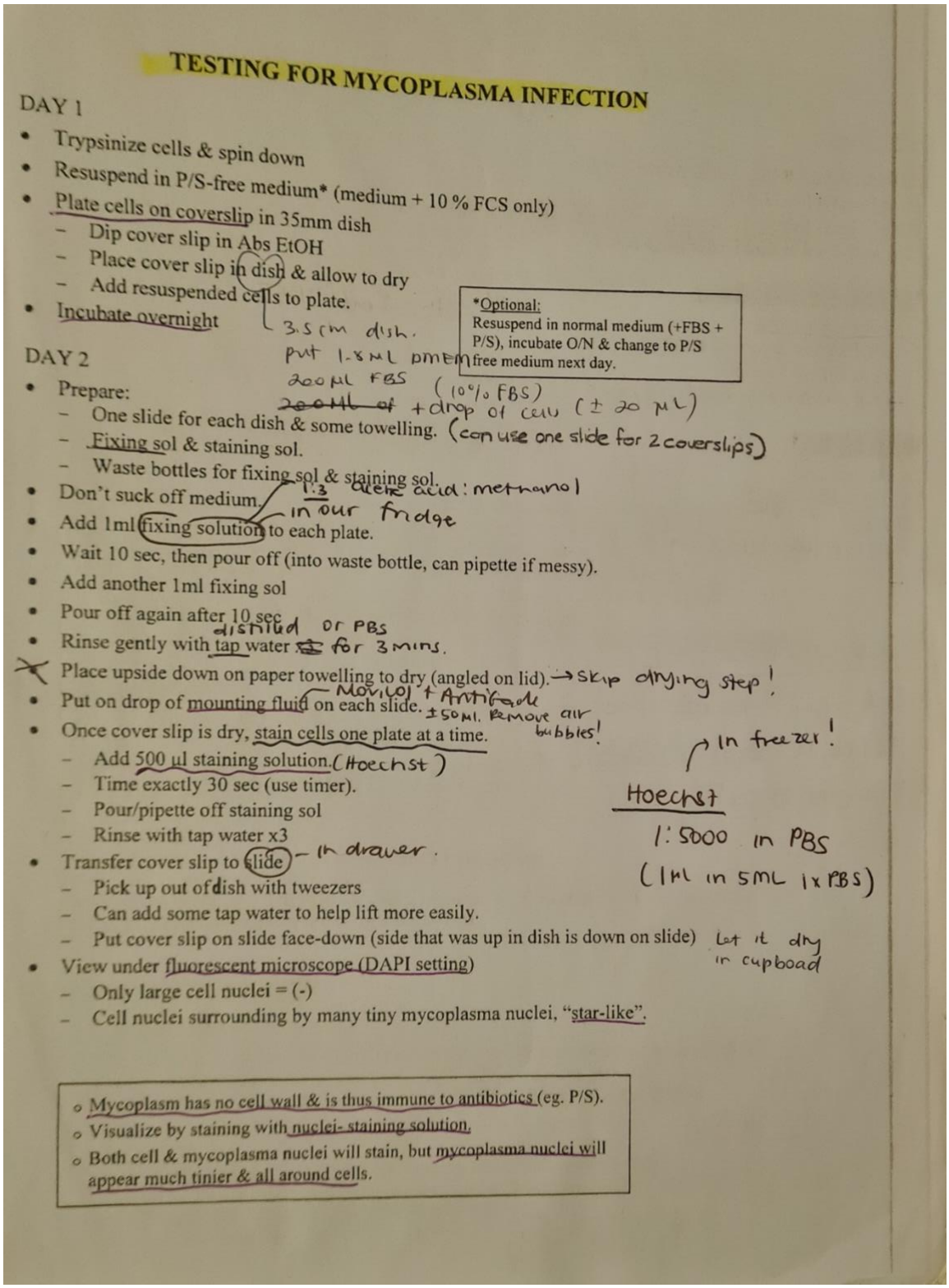

TESTING FOR MYCOPLASMA INFECTION

DAY 1

- Trypsinize cells & spin down
- Resuspend in P/S-free medium* (medium + 10 % FCS only)
- Plate cells on coverslip in 35mm dish
  - Dip cover slip in Abs EtOH
  - Place cover slip in dish & allow to dry
  - Add resuspended cells to plate.
- Incubate overnight

3.5cm dish.
Put 1.8ml DMEM
200µl FBS (10% FBS)
~~200ml of~~ + drop of cells (± 20 µL)

*Optional:
Resuspend in normal medium (+FBS + P/S), incubate O/N & change to P/S free medium next day.

DAY 2

- Prepare:
  - One slide for each dish & some towelling. (can use one slide for 2 coverslips)
  - Fixing sol & staining sol.
  - Waste bottles for fixing sol & staining sol.
- Don't suck off medium.
- Add 1ml fixing solution to each plate. (1:3 acetic acid : methanol, in our fridge)
- Wait 10 sec, then pour off (into waste bottle, can pipette if messy).
- Add another 1ml fixing sol
- Pour off again after 10 sec
- Rinse gently with tap water (distilled or PBS) ~~3~~ for 3 mins.

~~X~~ Place upside down on paper towelling to dry (angled on lid). → skip drying step!

- Put on drop of mounting fluid on each slide. (Mowiol + Antifade) ±50ml. Remove air bubbles!
- Once cover slip is dry, stain cells one plate at a time.
  - Add 500 µl staining solution. (Hoechst) → in freezer!
  - Time exactly 30 sec (use timer).
  - Pour/pipette off staining sol
  - Rinse with tap water x3
- Transfer cover slip to slide – in drawer.
  - Pick up out of dish with tweezers
  - Can add some tap water to help lift more easily.
  - Put cover slip on slide face-down (side that was up in dish is down on slide) Let it dry in cupboard
- View under fluorescent microscope (DAPI setting)
  - Only large cell nuclei = (-)
  - Cell nuclei surrounding by many tiny mycoplasma nuclei, "star-like".

Hoechst
1:5000 in PBS
(1ml in 5ml 1x PBS)

- Mycoplasm has no cell wall & is thus immune to antibiotics (eg. P/S).
- Visualize by staining with nuclei- staining solution.
- Both cell & mycoplasma nuclei will stain, but mycoplasma nuclei will appear much tinier & all around cells.

Fig A2. Image of Mycoplasma testing protocol used in this study.

Section B: Stem cell cardiac differentiation

1)

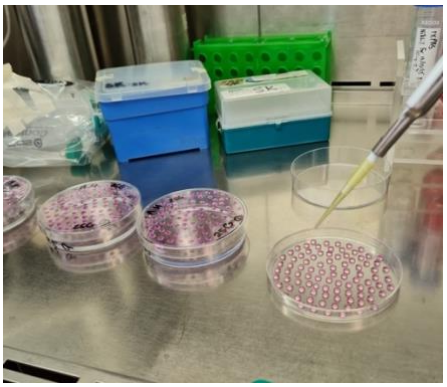

2)

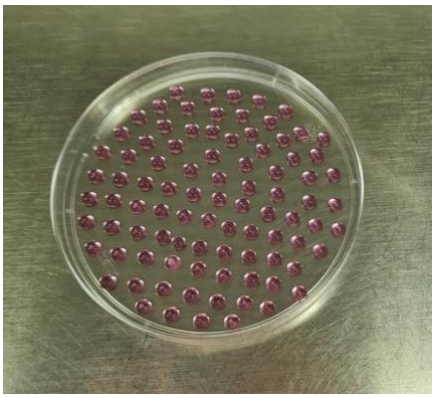

Fig B1 and B2. Image of EB formation by hanging drop method. Hanging droplets were made by forming rows of 20µL drops of the cell suspension (1000 cells/20μL drop) on the inner surface of a tissue culture dish. The lid was carefully inverted onto the culture dish and left undisturbed for 2 days in the incubator for EB formation to take place. Importantly, the glucose concentration used was labelled clearly on the lid (25 mM or 50 mM).

Section C: Experimental design and interventions

C1. Myocyter workflow

The following is a simplified workflow for the Myocyter™ program. A more detailed, step-by-step manual, as well as the latest version of Myocyter™, may be downloaded for free here: www.scyrus.de. In this study, version 1.3 was used.

Step 1

Convert all videos/time-lapse images into an ImageJ compatible format, preferably an uncompressed *.avi file. A frame rate of at least 60 frames/second is recommended.

Step 2

Open ImageJ, and then open the Myocyter™ macro either by dragging it and dropping it onto the ImageJ tab or going into ImageJ and clicking "Select"→"Macros"→"Run Macro". Press "Ctrl + R", and a user-interface should appear with a dropdown menu of options as shown below. Go straight to selection 3 (Region of interest/ROI selection).
Although Myocyter™ can automatically detect any beating areas within the EBs (i.e., Step 1: Pre-test movement), it is easier and more precise to manually outline your own beating cluster.

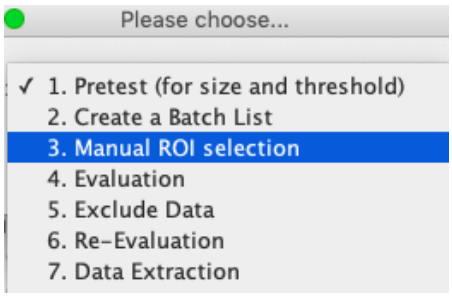

Step 3

Once you have selected "Manual ROI selection" and clicked "OK", you will then be asked to select the folder containing your time-lapse images in *.avi format. Once the file is open, the video will automatically start playing, allowing you to identify the beating areas you wish to analyse. Use one of the ImageJ selection tools to outline your ROI. The freehand drawing works quite well. Click "T" after each ROI has been selected. You will also be asked to select a reference frame for each ROI, against which all the other frames will be measures. Use the slider below the video to select frame. I found that if the EB beating area is in a relaxed state at the start of the video clip, I can use the very first frame as default. Otherwise, if the clip starts with the EB in mid-contraction, select a different frame. This will ensure that in the final graphical output, the contractions appear as upward facing tracings. Select "OK".

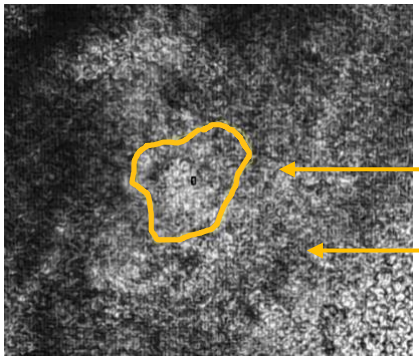

Step 4

Click “Ctrl + R”, and select step 4, which is evaluation. A menu will pop-up and you will have an opportunity to optimise various parameters such as the detection threshold (i.e., how small of an amplitude should the program recognise as an actual contraction vs background noise). For the most part, I leave all the settings at default, and this has worked very well. Importantly, check the option “use ROI-list” a shown below, then click “OK” to continue. You will now be asked to select the folder containing your video/.avi file, and then *within* that folder you will also have to select the newly created “mainrois” folder which contains the ROI data from step 3.

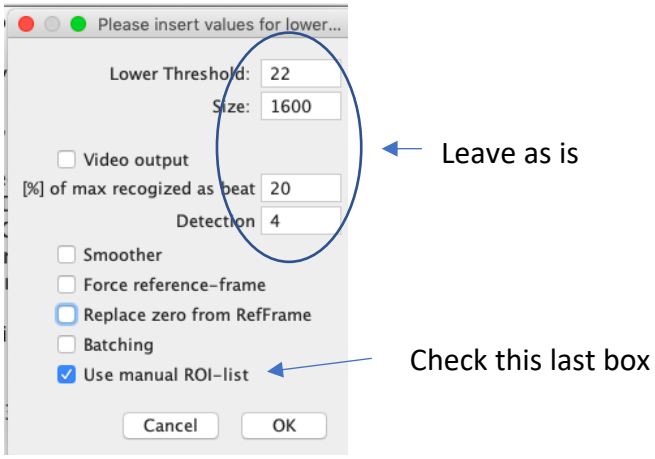

Menu with parameters to optimise prior to evaluation.

Step 5

The evaluation process may take several minutes (5 to 10), depending on the size of the file being processed. Do not use your computer during this period, the program will crash. Grab a coffee instead.

Step 6

Once the evaluation is done, a new folder ("Results") will be generated, containing several graphical and numerical data. A picture of the main graphical output is shown below:

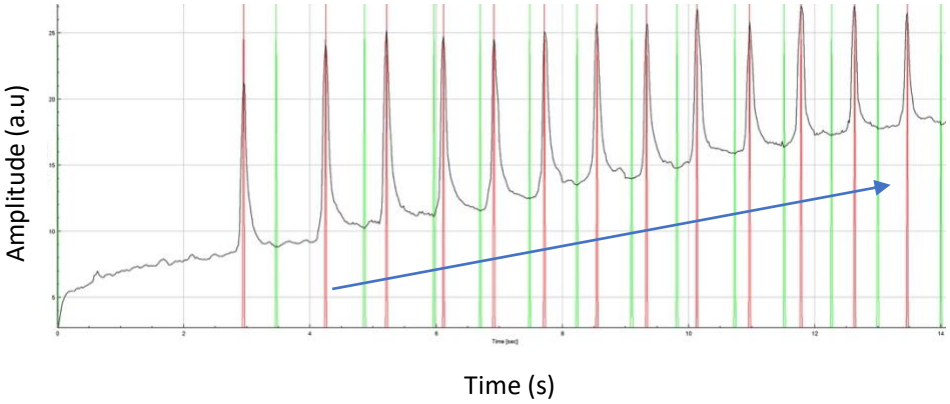

The vertical red lines indicate the peak of each detected contraction, and the green lines the troughs.

Myocyter™ also corrects for any shift of the amplitude along the y-axis as shown by the blue arrow. This process is known as "dynamic thresholding"

Step 7

Myocyter™ extracts up to 43 parameters, but for rate and rhythm analysis, only changes in Amplitude over time is needed. Go to the subfolder "diffMov" within the Results, then click "dataplots" and open the "Results.txt" file. Copy everything onto an Excel sheet, and then open a statistical software of your choice. In this study, OriginPro 6.1 (Origin®) was used. Copy only columns B ("Time") and D ("Baseline amplitude) from the Excel sheet into Origin®. Repeat for all the EBs, taking care to label each one correctly. From here, you can re-plot the original Myocyter™ tracings, perform further statistical analysis.

C2. Drug stimulation protocol

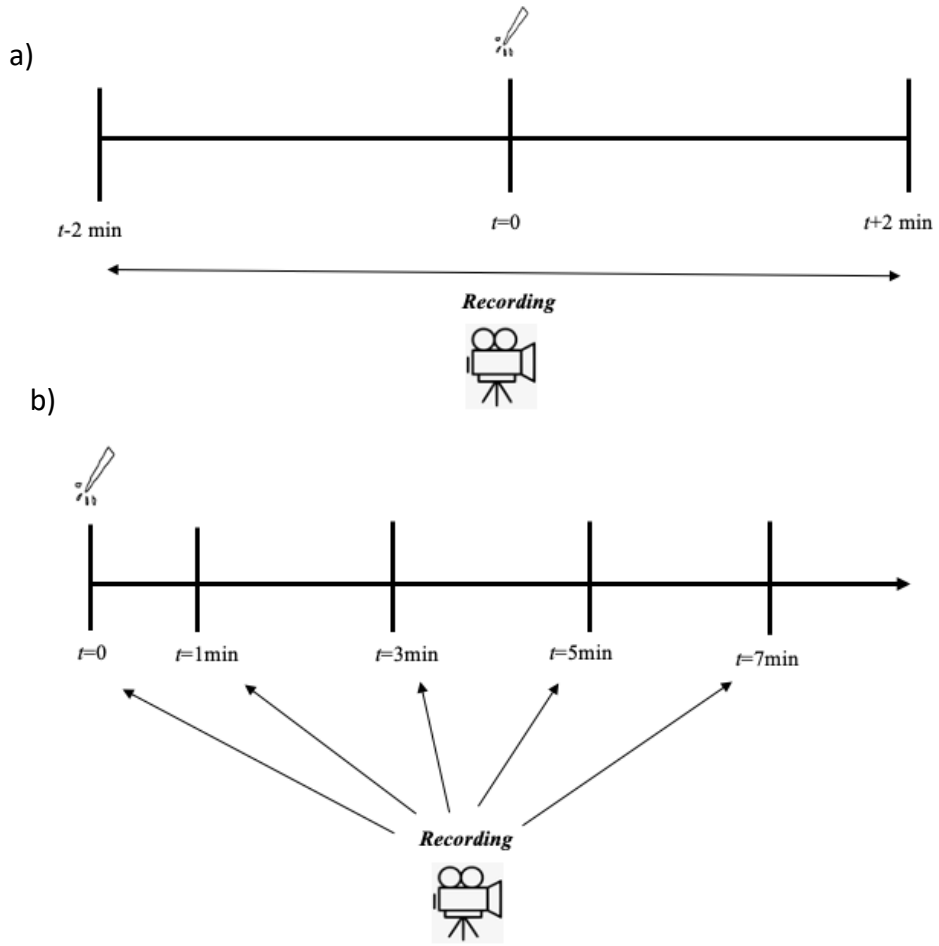

Fig c2. Schematic diagram of drug stimulation protocol. a) EBs were recorded for 2 minutes before and after application of either isoprenaline, ivabradine or KCl. b) EBs were recorded at 2-minute intervals following application of quinidine. The time interval during which asystole occurred was taken as the time to asystole.

C3. Western blot protocol

a)

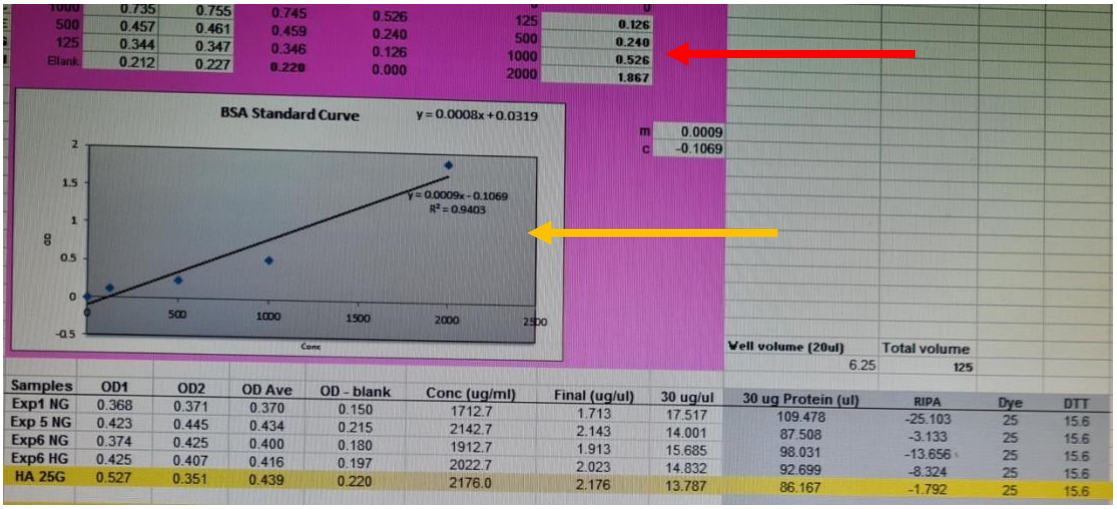

Samples	OD1	OD2	OD Ave	OD - blank	Conc (ug/ml)	Final (ug/ul)	30 ug/ul	30 ug Protein (ul)	RIPA	Dye	DTT
Exp1 NG	0.368	0.371	0.370	0.150	1712.7	1.713	17.517	109.478	-25.103	25	15.6
Exp 5 NG	0.423	0.445	0.434	0.215	2142.7	2.143	14.001	87.508	-3.133	25	15.6
Exp6 NG	0.374	0.425	0.400	0.180	1912.7	1.913	15.685	98.031	-13.656	25	15.6
Exp6 HG	0.425	0.407	0.416	0.197	2022.7	2.023	14.832	92.699	-8.324	25	15.6
HA 25G	0.527	0.351	0.439	0.220	2176.0	2.176	13.787	86.167	-1.792	25	15.6

Fig. C3a Protein quantification using standard curve. Absorbance of protein standards with known concentration measured using spectrophotometry. Optical density (OD) values inputted into this Excel spreadsheet (red arrow) and standard curve constructed (yellow arrow). By inputting the OD values of the samples, the protein concentration of each sample can then be calculated, as well as the amount of diluent required to achieve a desired concentration of 30μg/20mL.

b)

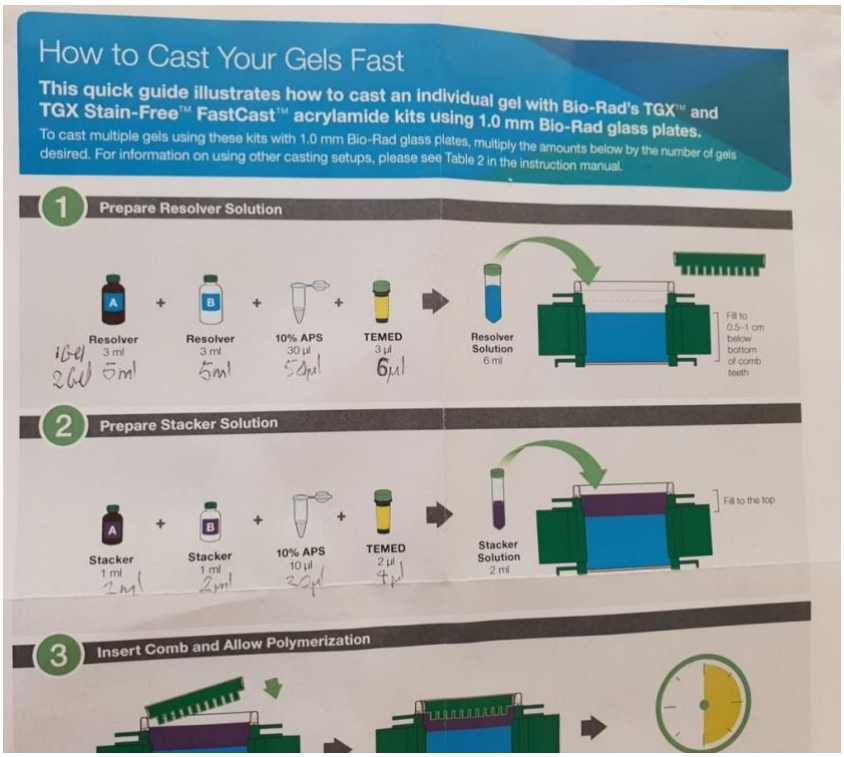

Fig. C3b SDS-polyacrylamide gels were prepared using the TGX FastCast™ acrylamide kit from Bio-Rad.

c)

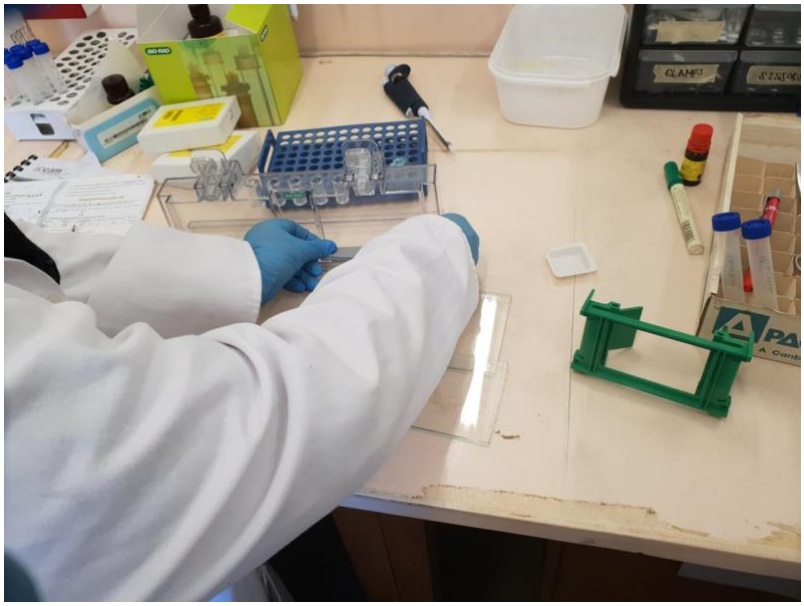

Fig. C3c Image of SDS-polyacrylamide gels being prepared as per protocol above.

d)

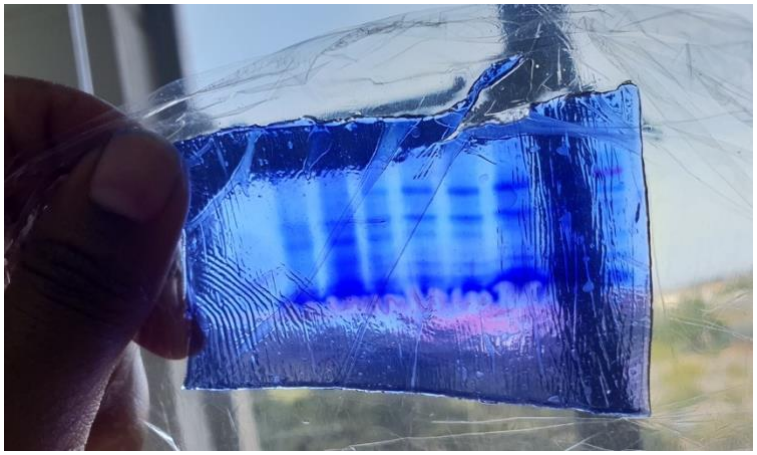

Fig. C3d Image of Coomassie Brilliant Blue staining of SDS-PAGE gel, showing protein bands in dark blue.

e)

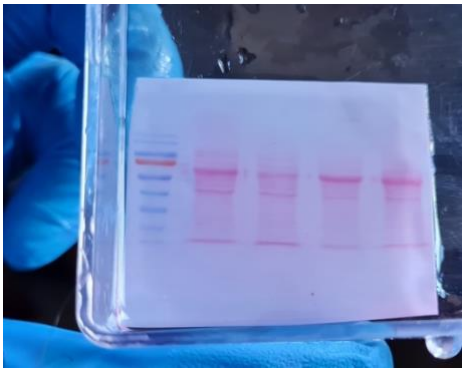

Fig. C3e Image of Ponceau staining of membrane to confirm successful protein transfer. Pink bands indicate presence of protein. The first lane has been loaded with protein ladder for determination of molecular weight.

C4. Scrape loading/dye transfer assay

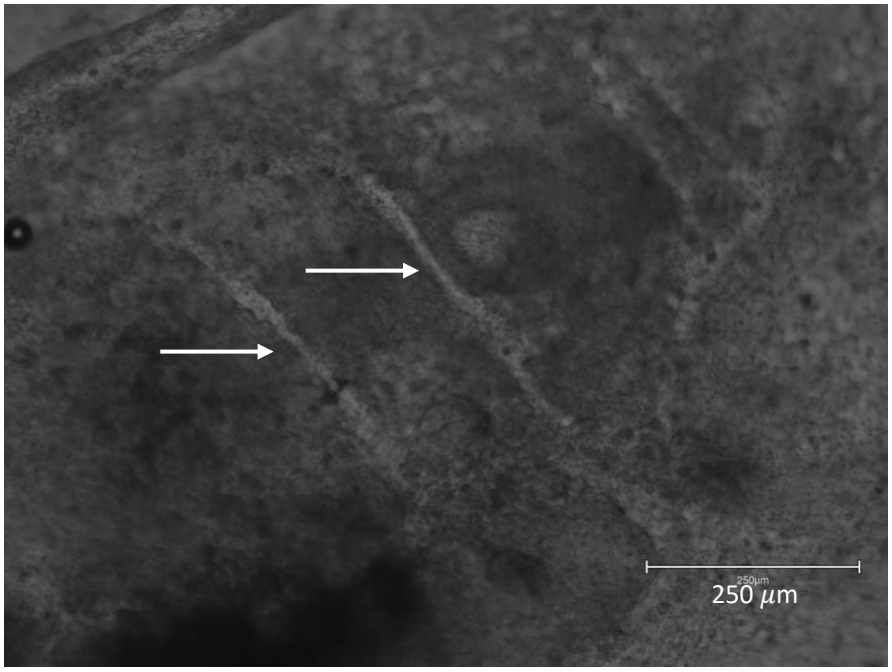

Fig. C4 Image of EB as viewed under 20X magnification on EVOS M500 microscope. White arrows indicate two clean cuts made across EB beating area using a surgical blade.

Western Blot protocol

A. Buffer Preparation

Buffers which need to be prepared include RIPA buffer, Tank Buffer, 1x PBS-T and 1X Transfer buffer.

RIPA: Take 5M NaCl and 1M Tris (pH 7.5) from the fridge and place on ice. Tris can also be made afresh, using HCl acid from the chemical shelf to achieve the desired pH. Get Triton X-100 from the Western Blot shelf. Weigh out 0.5g of deoxycholate powder. To make 10% SDS, weigh out 1g of SDS salt from WB shelf and add 10mL of dH_20 in a 15mL tube. Vortex and store at room temperature. Once all the reagents for RIPA buffer have been assembled, label a 50mL tube "RIPA Buffer" and add the date. This buffer can be stored at 4° for several months and used subsequently in sample preparation. Add the reagents according to the following table:

Reagent	Stock concentration	Final Concentration	For 50mL
NaCl	5M	150mM	1.5mL
Triton X-100	100%	1%	500uL
SDS	10%	0.1%	500uL
Tris (pH 7.5)		20mM	1mL
Deoxycholate	Powder	1%	0.5g
dH_20			46.5mL

Place on magnetic stirrer until all the deoxycholate powder has been completely dissolved and the solution is clear. Keep on ice.

Tank (Running) Buffer: Get the 10X TGS (Tris-Glycine-SDS) from the Western Blot cupboard and measure out 100mL, then pour into a labelled 1L container. Add 900mL of dH2O and keep the buffer at room temperature. New tank buffer should be prepared every 3 to 4 experiments, otherwise gel electrophoresis may run skew.

PBS-T: Fetch the Tween-20 from the WB shelf. Pour 50mL of 10X PBS (kept in box at room temperature) to a 500mL glass container. Add 450mL of dH_2O and 500uL of Tween. Place on magnetic stirrer for 10 to 15 minutes, then keep refrigerated when not in use.

Transfer Buffer: To make 4X Transfer Buffer, weigh out 43g of Tris base and 109.45g of Glycine. Make up to 2L with dH_2O. Label the container well. For 1x Transfer buffer, add 250mL 4x Transfer buffer and 200mL isopropanol, then make up to 1L with dH_2O. Keep at 4°C.

NB: There is ready-to-use Transfer Buffer from Bio-Rad currently available in the lab.

B. Tissue Harvesting and Homogenization

To make 1 sample for WB requires 7 to 10 EBs (preferably only those which are beating).

1. Put some PBS in the freezer ± 1 hour before starting as it must be ice-cold for the homogenization process.
2. Fetch Protease inhibitor and RIPA buffer from the fridge in the TC room (Hamida's white box) and keep on ice. There is also some PI in the lab on Level 3. See above for instructions on how to make RIPA buffer.
3. Get a 1mL syringe from the top drawer in TC room and keep it on ice as well.
4. Take out a centrifuge tube and fill it with some PBS (±10mL).
5. Fetch the cells from the incubator and view them under the microscope. Make a clear mark on the wells from which you wish to harvest beating EBs.
6. Aspirate the medium from the appropriate wells.
7. Add 1mL of the ice-cold PBS into each well
8. Take out 2 Eppendorf tubes, and in the first one, add: 300 to 400uL of RIPA, and 10uL of PI per 1mL of RIPA (e.g. if adding 300uL of RIPA, that will be 3uL of PI). Mix well with blue tip pipette. for 2x samples: 400 mL x 2 = 800 mL RIPA + 8 mL PI
9. If you have enough beating EBs to make more than 1 sample, then adjust accordingly (e.g. 600uL RIPA and 6uL of PI if making 2 samples).
10. Label the second Eppie with the name of your sample.
11. Remove the plunger of the syringe and let it soak in the centrifuge tube with the PBS (black rubber part facing down).
12. Aspirate the PBS from the wells.

13. With a blue tip pipette, take up the PI+ RIPA cocktail and add a little to each well (±50uL).
14. Use the syringe plunger (black rubber part) to gently scrub the cells in each well, and mix with the PI+ RIPA inside the well.
15. Once you've scrubbed the cells in every well, use a blue tip to suck up everything and transfer to the labelled eppie.
16. Keep the sample on ice, especially if preparing more than one.
17. Vortex for a few seconds.
18. Place the eppie in the 50mL tube with orange top (can be found in bottom drawer of TC room).
19. Place it on the blue roller (Robea) in the corridor fridge for 30 minutes.
20. After this, you may proceed with sample preparation or keep the sample at -20°C until you have more samples to work with. If proceeding with sample prep, then go immediately to Level 5 lab to start cooling the centrifuge to 4C°. This takes about 20 minutes. code: C14890

21. After the homogenization, centrifuge the samples for 30 minutes at 4°C and 15000g.

22. In the meantime, label new Eppendorf tubes with the sample names and carry the P200 pipette and tips to Vino Lab. After centrifuge, use the pipette to transfer the supernatants to new eppies and discard the pellet. Head back to the lab to prepare for the BCA assay.

C. BCA Assay

Take the BSA protein standards out of the freezer and thaw on ice. New standards can be made by following the Dilution Scheme which comes with the Pierce BCA kit. Transfer 10uL of each supernatant/sample to a new labelled Eppie, then dilute 1/6 with RIPA buffer (i.e. add 50uL of RIPA (*without* protease inhibitor) into each eppie. Calculate how much Working Reagent (WR) you will need: WR= (number of samples + number of BSA Standards) x2 for duplicates + 1 for pipetting error x 200uL for each well. This gives the volume for Reagent A. The ratio of reagent A to B in the WR is 50(A):1(B). Add A first then B, note the colour

change to green. Fetch a 96-well plate form the cupboard. Pipette 25ul of BSA standards into each well (in duplicates) followed by 25uL of diluted samples. Then, using a multichannel pipette, add 200uL of WR to each well. Note the colour change to purple. Remember to write down the order in which samples were added to the plate! Cover with parafilm and incubate at 37°C for 30 minutes.

Go to Sharon Prince Lab to use the plate reader, or use the older model in our lab. Measure absorbance at 560nm and email results to yourself. Using the Excel template on the computer desktop, create a BCA standard curve and fill in the O.D for your samples to obtain concentrations. Print this out and paste in work book to use for sample preparation.

D. Sample Preparation

Set the dry bath incubator to 95°C. Get 6X Dye and RIPA buffer from the fridge and DTT from -20°C and place on ice together with samples. Add the samples and RIPA according to the printed BCA standard curve, followed by 25uL of Dye and 15.6uL of DTT. Make sure all eppies are well labelled. Boil samples for 5 minutes, then briefly spin in Vino lab using desk centrifuge. Aliquot samples into Eppendorf tubes (e.g. 20uL or 40uL aliquots) and store at -20°C. If you are running an experiment on the same day, then keep samples on ice while you prepare gels for electrophoresis.

E. Gel Preparation

Gels can either be prepared from scratch using the TGX Fastcast Kit or precast gels can be used. For gel preparation (10%), clean the glass slides and short plates with 75% ethanol and tissue paper. Assemble the plates onto the gel-casting rack, then prepare the resolving gel solution using the Protocol pasted on the wall. For 2 gels, add 5mL of each solution (A and B). Then add 6uL of TEMED and 50uL of 10% APS. Vortex briefly and use a collapsible pipette to add the resolving solution to the appropriate level. Watch out for leaks. Add a layer of isopropanol to allow for polymerization. Leave for 15 minutes.

*If making gel from scratch: 40% Acrylamide is in brown bottle in fridge.

10% APS = 0.01g in 100 mL dH_2O

In the meantime, prepare the Stacking gel solution by adding 2mL of A and B. Do not add TEMED and APS just yet as this will start the polymerization immediately. At the end of the 15 minutes, use filter paper to remove the layer of isopropanol, then add TEMED and APS according to the protocol. If you find that you are experiencing problems with the stacking gel not polymerizing (perhaps the kit has expired), then increase the amount of APS to 30uL and TEMED to 5uL. Vortex briefly and add on top of the resolving gel. Place the comb in between the plates (avoid air bubbles) and allow to set for at least 20 minutes. If you are not using the gels immediately, wrap in clingfilm and store at 4°C for later use. Remember to take the gel out of the fridge 30 minutes before you intend to run electrophoresis.

F. Electrophoresis

Set the dry bath to 95°C. Take pre-made gels out of the fridge. After about 30 minutes, assemble the gels into the apparatus and fill the chamber with clean Tank buffer. Carefully remove the combs and rinse the wells with tank buffer using a collapsible pipette. Take samples out of the freezer and go boil for 5 minutes then briefly spin in Vino lab. If electrophoresis is being done immediately after sample preparation then there is no need to boil samples again. Take the protein ladder/MW marker out of the freezer. Place the sample loading guide on top of the 2 gels and load 20uL of each sample. If using the precast gels, there is no need to do this as the wells are clearly outlined and numbered. Fill up the space between the two gels to the brim with tank buffer, then connect the electrodes in the correct orientation. Switch on the power source and set to 150mV. Run for about 30-35 minutes or until the MW marker has separated adequately. In the meantime, take 1X Transfer buffer out of the fridge and cut out new squares of PVDF membrane (roughly 8x8 cm).

G. Transfer

During the last 15 minutes of the electrophoresis, pour transfer buffer into a ceramic bowl and soak 4 sets of filter paper. Pour methanol into a plastic container and using clean forceps, briefly submerge each PVDF membrane square for about 20 seconds, then allow them to equilibrate in the transfer buffer along with the filter papers.

Take the gels out of the electrophoresis chamber and carefully separate the glass plates to remove the gels. Make sure that the PVDF membrane squares are on top of a stack of filter paper, and smooth out any air bubbles with the roller. Place the gel on top of the membrane, then place the whole stack onto the transfer cassette. Adjust the membrane and gels so that they are not sticking out over the filter paper and smooth out any air bubbles. Complete the sandwich by adding the top stack of filter paper, then close the cassette and switch on the power source. Select "Turbo", which is a Mixed molecular weight 7-minute transfer program. This is useful if the proteins of interest are larger than 30kDa but smaller than 150kDa. For smaller proteins, go to List, then select BioRad followed by Low MW, and for large proteins select the High MW program. Clin on Run A and Run B if the 2 mini gels are in separate cassettes. If both mini gels are in the same cassette, make sure that you place then foot-to-foot and select "2 mini gels" instead of just 1.

During the transfer, clean up and pour transfer and tank buffers back into their respective containers. Take the Ponceau stain out of the fridge and into the dark room.

To test efficacy of transfer, you may choose to do Ponceau on just one half of the membrane or one lane, or perhaps the entire membrane. Once transfer has been completed, remove the membrane and cut out the piece to be stained. Place the rest of the membrane in an appropriately sized plastic container and briefly rinse with distilled water, then add blocking solution and set timer to 60 minutes.

For the Ponceau staining, take the portion of the membrane into the dark room and pour the stain over it. Cover and place on shaker for 5 minutes. After this, discard the ponceau stain and rinse vigorously with dH_2O until pink protein bands are visible. Take a picture for your own records, then wash the stain off for 3 x 10 minutes or until stain is no longer visible (with dH_2O). Proceed to blocking.

H. Blocking

Blocking is done for 1 hour at room temperature on the shaker. The blocking agent of choice may be 2% or 5% BSA or fat-free milk. This needs to be prepared well in advance. Add 100mL of PBS-T to a medium-sized glass jar. Weigh out 2g of BSA powder and pour into the

glass jar. Do not stir, just shake gently. Leave in the fridge for about 15 minutes and the BSA will spontaneously dissolve. Afterwards, filter the BSA using the syringe and single-use filter units (in black plastic container next to distilled water). Once filtered, use a collapsible pipette to pour blocking solution over the membrane. Pour enough to submerge the entire membrane. Leave for an hour. In the meantime, prepare primary antibody dilutions.

Note: Fat free milk (powder or fresh) is also an option, however 5% milk may result in significantly reduced signal, particularly for lowly expressed proteins. If BSA is unavailable, 2% fat free milk is the default.

I. Primary Antibody Incubation

Prepare the antibody dilution. It is simpler to dilute using the same agent used in the previous step (Blocking). This eliminates the need for a washing step. Take the primary antibody aliquot out of the freezer and briefly spin on desk centrifuge. Pour the appropriate volume of 2% BSA into a labelled tube and pipette the antibody into the tube. Gently mix by inverting the tube several times. At the end of the 60 minutes blocking time, pour out the blocking solution and use a collapsible pipette to add the primary antibody solution. Make sure to cover the membrane. Usually for half a membrane in a small container, 5mL is sufficient. Leave on shaker at 4°C (Level 6) overnight.

J. Secondary antibody incubation

The following day, fetch membranes from Level 6 and wash 3x 10 minutes with PBS-T. [Note: If BSA is used as a diluent, then then the primary antibody solution can be reused and does not have to be discarded]. In the meantime, prepare secondary antibody dilution. It is important to make sure that your primary and secondary antibodies are compatible. E.g. if Rabbit B-actin monoclonal Ab was used, then the appropriate secondary needs to be anti-rabbit (e.g. Goat-anti-rabbit). After the washing step, add the secondary antibody and leave on shaker at room temperature for 2 hours.

K. Detection

Discard the secondary antibody and wash the membranes for 3 x 10 minutes. In the meantime, prepare the dark room for detection. Prepare fresh developer solution by adding 100mL of developer stock to 500mL of dH20. Mix and pour out into the developing tub. Add fresh dH2O to the water tub, and make sure there is still enough fixing solution in the fixing tub. Switch off the Red light and cute a sheet of x-ray film into 3 or 4 smaller. Ensure that there is no light leaking into the dark room. Place the cut-out x-ray film pieces in the yellow envelope and keep hidden in cupboard until needed.

Mix the ECL reagents in a 1:1 ratio. For 2 membranes, 2mL of each reagent will be sufficient. Clean a transparency with 70% ethanol and allow it to dry. Place the flashy stickers under a lamp so that they absorb light. After the washing step, use forceps to remove the membrane and let the excess buffer drain onto a paper towel. Place the membrane onto the open transparency facing upwards, and place the transparency onto a cassette. Once in the dark room, use the collapsible pipette to drop ECL reagent onto the membrane and allow to stand for 60 to 90 seconds. The Quick Start protocol recommends 5 minutes; however, most protocols use 60 seconds. After this, close the transparency and remove excess reagent with a roller. Use tape to secure the sides of the transparency firmly onto the cassette to prevent movement when x-ray film is being removed. Place the flashy stickers at the molecular weight at which your protein of interest is expected, then seal the dark room and switch off the red light. In the dark, open the cupboard and take out a piece of x-ray film from the envelope. Fold one corner of it and place it carefully on top of the blot. Close the cassette and expose for 5 minutes to begin with. You may Place a large textbook on top of the closed cassette if you are struggling to obtain signal. After 5 minutes, open cassette, carefully remove the x-ray film by pulling on the folded corner and submerge in developer solution. Once submerged, turn on the red light so that you can see the appearance of bands. Once bands appear, briefly rinse the film in the water tub then submerge in fixer solution for 1 minute.

Repeat using different exposure. The ECL reagent is stable for an hour after it was prepared.

* strip + reprobe protocol *** on pg 72 of blue book 1 (Hons)